AD-751 804

AN ANALYTICAL SOLUTION OF THE COMPRESSIBLE LAMINAR MOMENTUM AND THERMAL BOUNDARY LAYERS WITH PRESSURE GRADIENT AND CONTINUOUS MASS INJECTION

R. E. Pavri, et al

Cincinnati University

PROJECT THEMIS REPORT NO. 72-29

AN ANALYTICAL SOLUTION OF THE
COMPRESSIBLE LAMINAR MOMENTUM AND
THERMAL BOUNDARY LAYERS WITH
PRESSURE GRADIENT AND CONTINUOUS
MASS INJECTION

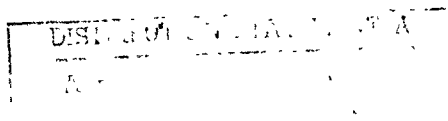R.E. Pavri and W. Tabakoff

September 1972

DEPARTMENT OF AEROSPACE ENGINEERING

University of Cincinnati, Cincinnati, Ohio 45221

DOCUMENT CONTROL DATA - R & D		
(Security classification of title, body of abstract and indexing annotation must be entered when the overall report is classified)		

1. ORIGINATING ACTIVITY (Corporate author)	2a. REPORT SECURITY CLASSIFICATION
University of Cincinnati	Unclassified
	2b. GROUP
	NA

3. REPORT TITLE

An Analytical Solution of the Compressible Laminar Momentum and Thermal Boundary Layers with Pressure Gradient and Continuous Mass Injection

4. DESCRIPTIVE NOTES (Type of report and inclusive dates)
Technical Report

5. AUTHOR(S) (First name, middle initial, last name)

R.E. Pavri and W. Tabakoff

6. REPORT DATE	7a. TOTAL NO. OF PAGES	7b. NO. OF REFS
September 1972	50	15

8a. CONTRACT OR GRANT NO.	9a. ORIGINATOR'S REPORT NUMBER(S)
DAHC04-69-C-0016	Project Themis Report No. 72-29
b. PROJECT NO.	
c.	9b. OTHER REPORT NO(S) (Any other numbers that may be assigned this report)
d.	AROD-T-4.47-E

10. DISTRIBUTION STATEMENT

Distribution of this report is unlimited

11. SUPPLEMENTARY NOTES	12. SPONSORING MILITARY ACTIVITY
None	U.S. Army Research Office - Durham Box CM, Duke Station Durham, North Carolina 27706

13. ABSTRACT

 The study describes an analytical solution of the nonsimilar laminar boundary layer with pressure gradient, variable wall temperature and continuous injection.

 The method consists of transforming the partial differential equations for momentum and enthalpy and then solving the transformed equations by assuming polynomial stream function and enthalpy profiles. Solutions obtained show very good agreement with exact numerical results.

 The solutions are obtained for flows over wedges as well as at the two-dimensional stagnation point and over curved surfaces of a two-dimensional body in crossflow. The results of the study show that the boundary layer is very strongly effected by the injection mass flow rate.

Key Words:

Transpiration Cooling

Thermal Boundary Layer with Pressure Gradient

Ia

TABLE OF CONTENTS

LIST OF ILLUSTRATIONS

LIST OF TABLES

NOMENCLATURE

Symbol	Description
a	Shear stress parameter
$(a)_i$	Coefficients of $(\eta)^i$ in expansion of f
$(b)_i$	Coefficients of $(\eta)^i$ in expansion of g
C_f	Friction factor, $\bar{\tau}/\frac{1}{2}\bar{\rho}\bar{u}^2$
C_p	Specific heat
$(d)_i$	Coefficients of $(\eta)^i$ in expansion of ω
$f(\xi,\eta)$	Nondimensional stream function
F	As in Equation (51)
$g(\xi,\eta)$	Nondimensional enthalpy
h	Heat transfer coefficient
H	Enthalpy
$(I)_n$	As in Equation (56)
k	Thermal conductivity
L	Reference length
ℓ	Constant in Equation (61)
N	Blowing parameter
p	Pressure
Pr	Prandtl number, $\bar{C}_p\,\bar{\mu}/\bar{k}$
R	Universal gas constant
Re	Reynolds number, $\bar{U}_o\bar{\rho}_o\bar{L}/\bar{\mu}_o$
St	Stanton number, $\bar{h}/\bar{C}_{p_o}\bar{\rho}_o\bar{U}_o$
T	Temperature
U	Velocity
u,v	Components of local velocity in s and y directions, respectively

Symbol	Description
w	Injection rate
(x,y)	Orthogonal coordinates
α	Wall enthalpy, H_w/H_e
Δ	Ratio of minor axis to major axis
ϵ	As given in Equation (66)
λ	Pressure gradient parameter
μ	Viscosity
$\omega(\xi,\eta)$	As in Equations (52) and (53)
ρ	Density
ψ	Stream function
τ	Shear stress
(ξ,η)	Transformed coordinates

Subscripts

c	Coolant conditions
e	Condition at the edge of the boundary layer
o	Reference conditions
w	Wall conditions
x	Based on local value of x
$(\ )_\xi$	Differentiation with respect to ξ
in	Initial values

Superscripts

$(\ )'$	Differentiation with respect to η

ABSTRACT

The study describes an analytical solution of the nonsimilar laminar boundary layer with pressure gradient, variable wall temperature and continuous injection.

The method consists of transforming the partial differential equations for momentum and enthalpy and then solving the transformed equations by assuming polynomial stream function and enthalpy profiles. Solutions obtained show very good agreement with exact numerical results.

The solutions are obtained for flows over wedges as well as at the two-dimensional stagnation point and over curved surfaces of a two-dimensional body in crossflow. The results of the study show that the boundary layer is very strongly effected by the injection mass flow rate.

INTRODUCTION

The concepts of transpiration cooling with the accompanying high efficiency is shielding a surface from severe thermal environment are well known and have been discussed at length in the literature. Critical temperatures and thermal environments are encountered in combustion chambers, over gas turbine blades and near the nose of a re-entry vehicle. Transpiration cooling perhaps finds its most important applications in keeping these components at an acceptable temperature.

The advantages of increased gas temperature on the performance of a gas turbine are well known. The increase in turbine entry temperature causes an almost monotonic rise in efficiency and specific power. On the other hand, this high temperature coupled with excessive centrifugal and gas bending stresses produce a critical situation in the gas turbines, especially over the first stage rotor blades. To insure efficient performance over a reasonably high lifetime makes the problem of blade cooling absolutely necessary.

In a previous report[1], the authors have described an analytical solution of the compressible laminar boundary layer over a flat plate with continuous or local mass injection. There, the authors showed that even a small injection rate (2% or less of the main flow) is very effective in lowering the plate wall temperature. Though high pressure gradients are present near the stagnation point and over the rest of the turbine blade, similar results are observed for this case also. For example, Gollnick[2] showed that transpiration cooling is sufficient for practical use in cooling the axisymmetric stagnation region of a re-entry vehicle. Goodwin and Howe[3] showed that for relatively low mass flow rate (0.1% to 1.0% of the main stream) the aerodynamic heating is shielded to a great extent. These solutions, however, are based on the principle of "similarity" and have to be viewed critically. In the presence of injection, the boundary layer is not likely to be similar. Various authors[4],[5],[6] have solved these non-similar boundary layers using analytical or numerical techniques. These analytical solutions predict nonsimilar boundary layer behavior well for uniform injection along a flat plate with constant fluid properties. However, these approaches breakdown in the presence of pressure gradients.

This study is an extension of the previous work[1] and incorporates the presence of pressure gradients in the laminar flow field. The report describes an analytical solution of the nonsimilar laminar boundary layer with continuous injection and variable wall temperature over a two-dimensional body in cross-flow. The method, which consists of transforming the partial differential equations of momentum and enthalpy and then solving them by assuming polynomial velocity and enthalpy profiles, is similar to the one described in the previous report[1].

The aerodynamic performance of the heavily loaded turbine blade necessitates that the mass flow rate of the coolant effusing from the blade surface be kept as low as possible. First, the low, transverse velocity of the injected coolant will cause a decrease in the kinetic energy of the mainstream through direct momentum exchange. Second, as shown in the first report, the injection in the laminar boundary layer makes the layer unstable and enhances the transition to turbulence. Consequently, the injection flow rate is to be kept as low as possible. In this study, the injection rate is assumed 1% or less of the main flow rate near the stagnation point and less than 5% over the rest of the body surface.

ANALYSIS

The equations of motion for a two-dimensional body in cross-flow are:

Continuity;

$$\frac{\partial}{\partial \bar{x}} (\bar{\rho}\bar{u}) + \frac{\partial}{\partial \bar{y}} (\bar{\rho}\bar{v}) = 0 \tag{1}$$

Momentum;

$$\bar{\rho}\bar{u} \frac{\partial \bar{u}}{\partial \bar{x}} + \bar{\rho}\bar{v} \frac{\partial \bar{u}}{\partial \bar{y}} = - \frac{\partial \bar{p}}{\partial \bar{x}} + \frac{\partial}{\partial \bar{y}} (\bar{\mu} \frac{\partial \bar{u}}{\partial \bar{y}}) \tag{2}$$

Energy;

$$\bar{\rho}\bar{u} \frac{\partial \bar{H}}{\partial \bar{x}} + \bar{\rho}\bar{v} \frac{\partial \bar{H}}{\partial \bar{y}} = \frac{\partial}{\partial \bar{y}} [\frac{\bar{\mu}}{Pr} \frac{\partial \bar{H}}{\partial \bar{y}} + \bar{\mu} (1 - \frac{1}{Pr}) \frac{1}{2} \frac{\partial \bar{u}^2}{\partial \bar{y}}] \tag{3}$$

Here it is assumed that the flow is subsonic. The total enthalpy $\bar{H}$ is given by

$$\bar{H} = \bar{C}_p \bar{T} + \frac{1}{2} \bar{u}^2 \tag{4}$$

2

If Prandtl number (Pr) is assumed to be unity, the energy equation reduces to

$$\bar{\rho}\bar{u}\,\frac{\partial \bar{H}}{\partial \bar{x}} + \bar{\rho}\bar{v}\,\frac{\partial \bar{H}}{\partial \bar{y}} \quad (\bar{\mu}\,\frac{\partial \bar{H}}{\partial \bar{y}}) \tag{5}$$

These equations are then nondimensionalized by introducing the expressions

$$x = \frac{\bar{x}}{L}, \quad y = \frac{\bar{y}}{L}\,\sqrt{Re_o}, \quad u = \bar{u}/\bar{U}_o, \quad v = \bar{v}\,\sqrt{Re_o}/\bar{U}_o,$$

$$\rho = \bar{\rho}/\bar{\rho}_o, \quad T = \bar{T}/\bar{T}_o, \quad p = \bar{p}/\bar{\rho}_o\,U_o{}^2, \quad \mu = \bar{\mu}/\bar{\mu}_o,$$

$$C_p = \bar{C}_p/\bar{C}_{p_o}, \quad H = \bar{H}/\bar{H}_o \tag{6}$$

Here

$$Re_o = \bar{\rho}\,\bar{U}_o\,\bar{L}/\bar{\mu}_o \tag{7}$$

The equations of motion then reduce to

$$\frac{\partial}{\partial x}\,(\rho u) + \frac{\partial}{\partial y}\,(\rho v) = 0 \tag{8}$$

$$\rho u\,\frac{\partial u}{\partial x} + \rho v\,\frac{\partial u}{\partial y} = -\,\frac{\partial p}{\partial x} + \frac{\partial}{\partial y}\,(\mu\,\frac{\partial u}{\partial y}) \tag{9}$$

$$\rho u\,\frac{\partial H}{\partial x} + \rho v\,\frac{\partial H}{\partial y} = \frac{\partial}{\partial y}\,(\mu\,\frac{\partial H}{\partial y}) \tag{10}$$

At the edge of the boundary layer, the pressure gradient is written as

$$-\,\frac{\partial p}{\partial x} = \rho_e\,u_e\,\frac{\partial u_e}{\partial x} \tag{11}$$

3

and the various thermodynamic and transport variables reduce to

$$\frac{T}{T_e} = \frac{H - \frac{1}{2} u^2}{H_3 - \frac{1}{2} u_e^2}$$

$$\frac{\mu}{\mu_e} = \frac{T}{T_e} \qquad , \qquad \frac{\rho_e}{\rho} = \frac{T}{T_e} \qquad (12)$$

Here a linear viscosity-temperature relationship is assumed.

It is convenient at this point to introduce the Lees-Dorodnitsyn transformation of coordinates.

$$\xi = \int_o^x \rho_e \mu_e u_e \, dx \qquad (13)$$

and

$$\eta = \frac{\rho_e \mu_e}{\sqrt{2\xi}} \int_o^y \frac{\rho}{\rho_e} \, dy \qquad (14)$$

The stream function ψ is defined as

$$\frac{\partial \psi}{\partial x} = - \rho v \qquad \text{and} \qquad \frac{\partial \psi}{\partial y} = \rho u \qquad (15)$$

and is assumed to have the form

$$\psi = \sqrt{2\xi} \, f(\xi, \eta) \qquad (16)$$

From Equations (14), (15) and (16)

$$\frac{u}{u_e} = f'(\xi, \eta) \qquad (17)$$

where ( )' denotes differentiation with respect to η

4

An enthalpy function is defined as

$$\frac{H}{H_e} = g \tag{18}$$

The transformed fundamental equations obtained from the above relations are now written as

$$f''' + ff'' = 2\xi \left[f' \frac{\partial f'}{\partial \xi} - f'' \frac{\partial f}{\partial \xi} \right] + \lambda (g - f'^2) \tag{19}$$

and

$$g'' + fg' = 2\xi \left[f' \frac{\partial g}{\partial \xi} - g' \frac{\partial f}{\partial \xi} \right] \tag{20}$$

where

$$\lambda = - \frac{2\xi}{u_e} \frac{du_e}{d\xi} \tag{21}$$

BOUNDARY CONDITIONS

The boundary conditions in the physical plane are

$$\bar{y} = 0 \quad \begin{cases} \bar{u} = 0 \\ (\bar{\rho}\bar{v})_w = \bar{w} = \text{constant} \\ \bar{k} \frac{\partial \bar{T}}{\partial \bar{y}} = (\bar{\rho}\bar{v})_w \bar{C}_p (T_w - T_c) \end{cases} \tag{22}$$

$$\bar{y} \to \infty \quad \begin{cases} \bar{u} = U_e \\ \bar{T} = \bar{T}_e \end{cases} \tag{23}$$

Third condition of Equation (22) means that all the heat transferred from the hot gas goes to increase the coolant temperature to the exit wall temperature. In terms of the transformed variables, these boundary conditions reduce to,

5

$$\eta = 0 \quad \begin{cases} f' = 0 \\[2mm] f_w = - \dfrac{w \sqrt{Re_o}}{\rho_e \mu_e \sqrt{2\xi}} \int_o \dfrac{d\xi}{u_e} \\[4mm] \dfrac{\partial g}{\partial \eta} = \dfrac{\sqrt{2\xi} \, w \sqrt{Re_o}}{u_e} (g_w - g_c) \end{cases} \qquad (24)$$

$$\eta \to \infty \quad \begin{cases} f' = 1 \\[2mm] g = 1 \end{cases} \qquad (25)$$

The second condition of Equation (24) is derived from the definition of the stream functions, Equations (15) and (16). For flow over wedges where the pressure gradient (λ) is constant, U_e can be written as an explicit function of ξ. In that case, the value of f_w can be obtained as an explicit function of ξ. However, for flow over curved surfaces, pressure gradient varies with the downstream distance and hence it is much easier to obtain the value of f_w at each point (ξ) by numerically carrying out the integration up to that location.

SOLUTION OF THE NONSIMILAR EQUATIONS

The solution of the nonsimilar Equations (19) and (20) is obtained in a manner analogous to that described in the previous report[1]. The modified stream, and the enthalpy function are expanded in terms of polynomials of η:

$$f = N + \sum_{n=1}^{9} \frac{a_n \eta^n}{n!} \qquad (26)$$

$$g = g_w + \sum_{n=1}^{7} \frac{b_n \eta^n}{n!} \qquad (27)$$

where a_n and b_n are functions of ξ only.

From previous work[1],[7] it was realized that to obtain a reasonably good accuracy near the two-dimensional stagnation point ($\lambda = -1.0$), it is necessary to include at least 10 terms in the

stream function. It was also observed[7] that the momentum equation is much more sensitive and unstable than the energy equation. Consequently, terms up to η^8 are included in the momentum equation while energy equations retain terms only up to η^6.

If all the terms present in the coefficients of powers of η are retained, the solution becomes very lengthy and cumbersome. Hence, an order of magnitude analysis is necessary to retain only the most significant terms.

From the boundary conditions at $\eta = 0$ and from direct differentiation of the Equations (26) and (27) it follows

$$a_1 = 0 \qquad\qquad (28)$$

$$N = f_w \qquad\qquad (29)$$

$$b_1 = \left.\frac{\partial g}{\partial \eta}\right|_{\eta=0} \qquad\qquad (30)$$

Again, following the procedure described for the flat plate solution, the unknown coefficients a_3, a_4; b_2, b_3 etc. are obtained in terms of a_2, N and g_w by substituting Equations (26) and (27) into Equations (19) and (20) and matching the coefficient of powers of η.

Since the injection mass flow rate is kept 1% or less (of the main flow), the absolute value of N, especially near the stagnation point turns out to be always less than 0.7. In that case, the contribution of all terms involving N in a_7, a_8, a_9 and b_6 and b_7 is quite small as compared to the contribution of the terms present in a_2 to a_6 and b_1 to b_5. Hence all terms involving N are neglected in the expression of a_7, a_8, a_9, b_6 and b_7. Again, only first and second order terms in N are retained in a_6 and b_5. Also, since the values of $\xi\, da/d\xi$, $\xi\, dg_w/d\xi$, $\xi\, dN/d\xi$, b_2 etc. are the same order of magnitude (or less) as N, the same assumptions are applied to these terms or a product of these terms. These assumptions greatly simplify the final solution. Further comments on these assumptions are made in later chapters.

The various coefficients are obtained as

$$a_2 = a = \text{unknown} \qquad\qquad (31)$$

$$a_3 = - Na - 2\xi\, a(N)_\xi + \lambda\, \alpha \qquad\qquad (32)$$

$$a_4 = N^2 a - 4\xi aN(N)_\xi + 4\xi^2 a(N)_\xi^2 - N\lambda\alpha + b_1\lambda - 2\xi\lambda\alpha(N)_\xi$$

$$(33)$$

$$a_5 = -N^3 a - 6\xi aN^2(N)_\xi - 12\xi^2 aN(N)_\xi^2 - a^2 + 2\lambda(a)_\xi - 8\xi^3 a(N)_\xi^3$$

$$+ \lambda N^2\alpha - b_1 N\lambda + 4\xi\lambda\alpha N(N)_\xi - 2\lambda a^2 - 2\xi b_1\lambda(N)_\xi + b_2\lambda$$

$$+ 4\xi^2\lambda\alpha(N)_\xi$$

$$(34)$$

$$a_6 = -Na_5 - 4a_3 a + \lambda b_3 - 6\lambda a a_3 - 2\xi(N)_\xi a_5 + 4\xi a(a_3)_\xi$$

$$(35)$$

Neglecting all terms of the order of N^3 or higher and substituting the values of a_3, a_5, b_3, etc.

$$a_6 = 3N^2 b_1\lambda + 5Na^2 + 8\lambda Na^2 - 6\xi aN(a)_\xi + 12\lambda b_1 N\xi(N)_\xi$$

$$- 4a\lambda\alpha + 2\xi a\lambda(\alpha)_\xi + 12\xi^2 b_1\lambda(N)_\xi^2 - 4\xi^2 a(N)_\xi(a)_\xi$$

$$+ 16\lambda a^2\xi(N)_\xi - 6\lambda^2 a\alpha + 4\xi a\alpha(\lambda)_\xi + 6a\xi\lambda(\alpha)_\xi$$

$$- 2 a^2\xi(N)_\xi - 8\xi^2 a(a)_\xi(N)_\xi$$

$$(36)$$

$$a_7 = -Na_6 - 7aa_4 - 4(a_3)^2 + \lambda b_4 - 6\lambda(a_3)^2 - 8\lambda aa_4$$

$$+ 6\xi a(a_4)_\xi - 2\xi a_4(a)_\xi + 2\xi a_3(a_3)_\xi - 2\xi a_6(N)_\xi$$

$$(37)$$

This reduces to

$$a_7 = -8ab_1\lambda - 4\lambda^2\alpha^2 - 6\lambda^3\alpha^2 - 8\lambda^2 ab_1$$

$$(38)$$

Similarly, expressions for a_8 and a_9 are

$$a_8 = -16\lambda^2 b_1 \alpha + 32a^3\lambda + 20a^3\lambda^2 + 11a^3 - 20\lambda^3 b_1 \alpha \tag{39}$$

$$a_9 = 90a^2\lambda\alpha + 226\lambda^2 a^2\alpha - 16b_1^2\lambda^2 - 20b_1^2\lambda^3 + 132\lambda^3 a^2\alpha \tag{40}$$

Here

$$\alpha = g_w . \tag{41}$$

$$b_1 = \left.\frac{\partial g}{\partial \eta}\right|_{\eta=0} \tag{42}$$

$$b_2 = -Nb_1 - 2\xi b_1 (N)_\xi \tag{43}$$

$$b_3 = N^2 b_1 + 4\xi N b_1 (N)_\xi + 2a(\alpha)_\xi \xi + 4\xi^2 b_1 (N)_\xi^2 \tag{44}$$

$$b_4 = -ab_1 - N^3 b_1 - 6N^2 b_1 (N)_\xi \xi - 4\xi N a (\alpha)_\xi$$

$$\quad - 12\xi^2 N b_1 (N)_\xi^2 + 4\xi a (b_1)_\xi - 8\xi^2 a (\alpha)_\xi (N)_\xi \tag{45}$$

$$\quad - 2\xi b_1 (a)_\xi - 8\xi^3 b_1 (N)^3 + 2\xi\lambda\alpha (\alpha)_\xi \tag{46}$$

$$b_5 = 5ab_1 N - 16\xi a N (b_1)_\xi - 4\xi N\lambda\alpha (\alpha)_\xi - \lambda\alpha b_1$$

$$\quad + 10\xi b_1 N (a)_\xi + 14\xi a b_1 (N)_\xi + 6\xi\lambda\alpha (b_1)_\xi$$

$$\quad - 16\xi^2\lambda\alpha (\alpha)_\xi (N)_\xi - 48\xi^2 a (b_1)_\xi (N)_\xi + 28\xi^2 (a)_\xi b_1 (N)_\xi$$

$$\quad - 2\xi b_1 \alpha (\lambda)_\xi + (\alpha)_\xi \{6\xi N^2 a + 56\xi^3 a (N)_\xi^2 + 40\xi^2 a N (N)_\xi\} \tag{47}$$

Similarly,

$$b_6 = -b_1^2\lambda \tag{48}$$

9

and

$$b_7 = 11b_1a^2 + 2b_1\lambda a^2 \tag{49}$$

All other terms in $b_.$ and b_7 are small in comparison to the above terms and are neglected.

The momentum equation, after first integration is written as

$$f'' = e^{-F} \omega(\xi,\eta) \tag{50}$$

where

$$F = \int_o^\eta f \, d\eta \tag{51}$$

and

$$\omega(\xi,\eta) = \int_o^\eta [2\xi\{f'(f')_\xi - f''(f)_\xi\} + (g - f'^2)] e^F \, d\eta + a \tag{52}$$

Now $\omega(\xi,\eta)$ is expanded in terms of powers of η as

$$\omega(\xi,\eta) = \sum_o^\infty \frac{d_n \eta^n}{n!} \tag{53}$$

Equations (26) and (53) together with the well known expansion of the exponent

$$e^{-F} = 1 - F + \frac{F^2}{2!} + \text{----------- etc.} \tag{54}$$

are then substituted into Equation (50). Again, matching the coefficients of powers of η gives the coefficients "d_n" in terms of a, α and N.

A second integration reduces Equation (50) to

$$f'(\xi,\eta) = \int_o^\eta e^{-F} (\sum_o^\infty \frac{d_n \eta^n}{n!}) \, d\eta \tag{55}$$

As shown elsewhere[1], this equation can be written as

$$f'(\xi,\eta) = \int_o^\eta e^{-\frac{a\eta^3}{6}} \left(\sum_{n=0}^{8} I_n \eta^n \right) d\eta \tag{56}$$

Here the right hand side is expanded up to the eighth power of η. I_n are functions of d_n and hence functions of a, α and N.

By setting the upper limit to $\eta = \infty$ gives the left hand side as

$$f'(\xi,\infty) = 1.0 \tag{57}$$

(This follows from the remaining boundary condition.) Thus, when the integration is performed and the numerical values of the Gamma functions substituted, the final solution of the momentum equation is obtained as

$$a^{2/3} [C_o + \frac{1}{720} C_6 - \lambda(\frac{1}{3} C_3 + \frac{1}{90} C_6) + \frac{1}{36} C_6 \lambda^2] + a^{1/3}[N(-C_1 + \frac{1}{24} C_4$$

$$+ \frac{1}{3} \lambda C_4) + \xi(N)_\xi (-2C_1 - \frac{5}{12} C_4 + \frac{2}{3} \lambda C_4)] + [2 C_2 \xi^2 (N)_\xi^2$$

$$+ 2 C_2 \xi N (N)_\xi + \frac{1}{2} C_2 N^2] + a^{-1/3}[\frac{1}{3} C_3 \xi(a)_\xi - \frac{1}{360} C_6 \xi(a)_\xi$$

$$- \frac{4}{3} C_3 \xi^3 (N)_\xi^3 - 2 C_3 \xi^2 N (N)_\xi^2 - C_3 N^2 (N)_\xi - \frac{C_3}{6} N^3]$$

$$+ a^{-2/3}[\alpha(\lambda C_1 - \frac{1}{4} \lambda^2 C_4) + \frac{1}{4} C_4 \xi \lambda (\alpha)_\xi + \alpha C_7 (\frac{\lambda}{252} + \frac{\lambda^2}{315} + \frac{5}{191} \lambda^3)$$

$$- \frac{1}{4} C_4 N \xi(a)_\xi - \frac{1}{2} C_4 \xi^2 (N)_\xi (a)_\xi + \frac{1}{6} C_4 \xi \alpha (\lambda)_\xi] + a^{-1}[\alpha(0.5 C_2 N \lambda$$

$$- C_2 \xi \lambda (N)_\xi + \frac{1}{20} C_5 N \lambda + \frac{11}{60} C_5 \xi \lambda (N)_\xi + \frac{1}{4} C_5 N \lambda^2) + b_1 (\frac{1}{2} C_2 \lambda + \frac{1}{60} C_5 \lambda$$

$$- \frac{1}{15} C_5 \lambda^2) - \frac{1}{4} C_5 \xi N \lambda (\alpha)_\xi + \frac{1}{6} \xi N C_5 \alpha (\lambda)_\xi] + a^{-4/3}[\alpha(\frac{1}{6} C_3 \lambda N^2$$

$$+ \frac{2}{3} C_3 N \xi \lambda (N)_\xi + \frac{2}{3} C_3 \xi^2 \lambda (N)_\xi^2) + b_1 (- \frac{1}{3} C_3 N \lambda - \frac{2}{3} C_3 \xi \lambda (N)_\xi$$

$$+ \frac{1}{144} C_6 N \lambda + \frac{1}{15} C_6 \xi \lambda (N)_\xi + \frac{1}{15} C_6 N \lambda^2)] + a^{-5/3}[b_1 (\frac{1}{8} C_4 N^2 \lambda$$

$$+ \frac{1}{2} C_4 \lambda \xi N(N)_\xi + \frac{1}{2} C_4 \xi^2 \lambda (N)_\xi^2)] + a^{-2} [\alpha^2 (\frac{C_8 \lambda^2}{1260} - \frac{C_5 \lambda^2}{30} - \frac{C_5 \lambda^3}{20}$$

$$+ \frac{17}{2520} C_8 \lambda^3 + \frac{7}{840} \lambda^4 C_8] + a^{-7/3} [\frac{13}{240} C_6 N \lambda^2 \alpha^2 - \frac{1}{45} C_5 b_1 \lambda^2 \alpha$$

$$+ \frac{7}{120} \xi \lambda^2 \alpha^2 (N)_\xi + \frac{1}{120} C_6 N \lambda^3 \alpha^2] \tag{58}$$

where $C_0 = 1.623$, $C_1 = 1.493$, $C_2 = 2.0$, $C_3 = 3.234$, $C_4 = 3.73$, $C_5 = 12.0$, $C_6 = 25.92$, $C_7 = 59.6$ and $C_8 = 144.0$.

As shown by Meksyn[8], the solution of the momentum equation, Equation (58), may or may not be convergent depending on the number of terms involved and the value of λ. Setting $N = (N)_\xi = (a)_\xi = (\alpha)_\xi = 0$ and $\alpha = 1$, it is possible to evaluate the values of "a" for various values of λ. These values are presented in Table I.

Table I

Values of Shear Stress Parameter as a Function of λ (from Equation (58))

λ	a_{Lt} Literature Values	a_{pr} without Euler Transformation	a_{pr} with Euler Transformation
-1.0	1.232	1.31	1.234
-0.5	0.927	0.94	0.933
-0.2	0.687	0.696	0.694
-0.1	0.587	0.592	0.588
0	0.47	0.48	0.481

Comparing the values of a_{pr} (without Euler transformation from Table I and from previous work (1),(7) at $\lambda - 1.0$, it is evident that at that point the solution is very slowly converging.

Meksyn[8] has shown that this is due to the limited radius of convergence of Equation (53). To improve the convergence, Meksyn applies the Euler Transformation.

It is necessary to realize that the expression for $\omega(\xi,\eta)$, Equation (52) itself, is convergent. It is the transformed series, Equation (53) that is very slowly converging. As shown by Euler, the sum of this very slowly converging series is the finite numerical value of the convergent expression, Equation (52). A detailed account of the Euler transformation is given by Bromwich and Macrobert[9], Hardy[10] and Knopp[11]. Applying Euler transformation to the present solution, the values of the coefficients become $C_0 = 1.621$, $C_1 = 1.464$, $C_2 = 1.82$, $C_3 = 2.41$, $C_4 = 2.98$, $C_5 = 3.05$, $C_6 = 2.33$, $C_7 = 1.163$ and $C_8 = 0.281$. Substituting these values in Equation (58) and again setting $N = (N)_\xi = (a)_\xi = (\alpha)_\xi = 0$ and $\alpha = 1$, the values of "a" as as a function of λ are re-evaluated. These values are also shown in Table I. These values of "a" obtained with Euler transformation agree extremely well with the literature values.

In any case, from Table I, it can be concluded that the Euler transformation gives significant improvements only for high values of λ, i.e., near $\lambda = -1.0$. For cases where λ lies between $\lambda = 0$ and $\lambda = -0.7$, the solution of the momentum Equation (58), is convergent and the improvement caused by the Euler transformation is small.

As will be seen later, final solution of the momentum equation is obtained with, as well as, without the Euler transformation. Comparison between these two solutions is made in the chapter "Results and Discussion".

Solution of the energy equation is obtained along similar lines, with the final solution being

$$4\xi(\alpha)_\xi + a^{-1/3}[1.659b_1 + 0.072b_1\lambda - 6.476N\xi(\alpha)_\xi$$

$$- 4.312\xi^2(\alpha)_\xi(N)_\xi + 5.036\xi(b_1)_\xi]$$

$$+ a^{-2/3}[- 3.97N(b_1)_\xi + \xi(\alpha)_\xi(1.49N^2 + 8.945N(N)_\xi$$

$$+ 13.92\xi^2(N)_\xi^2) - 11.92\xi^2(b_1)_\xi(N)_\xi - 2.986\xi b_1(N)_\xi - 1.245Nb_1$$

$$+ 0.496\xi b_1\lambda(N)_\xi] + a^{-1}[4\xi^2b_1(N)_\xi^2 + 4\xi Nb_1(N)_\xi + b_1N^2]$$

$$+ a^{-4/3}[2.518\lambda\xi\alpha(\alpha)_\xi - 2.589\xi b_1(a)_\xi] + a^{-5/3}[-0.248\lambda b_1\alpha + 2.432\xi Nb_1(a)_\xi$$

$$- 0.993\xi N\lambda\alpha(\alpha)_\xi + 1.49\xi\lambda\alpha(b_1)_\xi - 3.97\xi^2\lambda\alpha(\alpha)_\xi(N)_\xi + 6.95\xi^2b_1(N)_\xi(a)_\xi$$

$$- 0.497\zeta b_1\alpha(\lambda)_\xi] + a^{-2}[-0.6b_1\alpha\lambda N - 0.1b_1^2\lambda - 3N\lambda b_1\alpha(1 + \lambda)/2$$

$$+ N\xi b_1 \alpha(\lambda)_\xi + 0.2b_1\xi\lambda\alpha(N)_\xi] + a^{-7/3}[0.288b_1^2N\lambda + 0.144\xi\lambda b_1^2(N)_\xi] = 1 - \alpha$$

$$(59)$$

Regardless of the number of terms involved or the value of λ, Equation (59) will always give $\alpha = 1.0$ at the stagnation point for $N = 0$. Hence, Euler transformation is not applied to the solution of the energy equation.

Conditions at the Stagnation Point

To solve the Equations (58) and (59) simultaneously it is necessary to have the initial values of "a" and α i.e., a_{in} and α_{in}. These initial values are also stagnation point values. There are two sets of stagnation point values depending on the mode of injection.

(i) If the injection is assumed to occur from $x > 0$, the stagnation values of a are the same as those given in Table II, i.e., for $\lambda = -1.0$,

$$a_{in} = 1.234 \qquad \text{(with Euler transformation)}$$

$$a_{in} = 1.31 \qquad \text{(without Euler transformation)}$$

and

$$\alpha_{in} = 1.0$$

(ii) If the injection is assumed to occur at the stagnation point, the problem can be resolved as follows.

Very near the stagnation point, the velocity outside the boundary layer of a two-dimensional body in crossflow can be written as

$$U_e = \ell x \tag{60}$$

where ℓ is a constant.

For a two-dimensional elliptic cylinder in crossflow,

$$\ell = \frac{1 + \Delta}{\Delta^2} \tag{61}$$

14

where Δ is the ratio of minor axis to major axis. From the definition of ξ, and Equation (60),

$$\xi = \frac{\ell}{2} x^2 \tag{62}$$

Again, for very small values of ζ, $\xi da/d\xi$, $\xi d\alpha/d\xi$ and $\xi dN/d\xi$ are neglected. Then,

$$f_w = - w\sqrt{\frac{Re_o}{\ell}} = N \tag{63}$$

Equation (63) then gives the stagnation value of N. The stagnation point values of "a" and α can now be obtained from simultaneous solution of Equations (58) and (59) using Equations (60) and (63). As mentioned above, $\xi da/d\xi$, $\xi d\alpha/d\xi$, $\xi d\lambda/d\xi$ and $\xi dN/d\xi$ are omitted. Under these assumptions, the solution reduces to "similar solution". However, at the stagnation point the value of $\xi \to 0$ and the nonsimilar terms tend to drop out.

Since the factor $f_w(N)$ incorporates the main flow rate, body geometry and the injection flow rate, the stagnation point solutions obtained with this factor as a parameter would constitute a very "general" solution. That is, such solutions would apply to any two-dimensional body in crossflow. The stagnation point values are given in Table II.

Table II

λ	$-f_w$	a	$(1 - \alpha)/(1 - \alpha_c)$
-1.0	0.0707	1.16	0.113
-1.0	0.212	1.02	0.299
-1.0	0.354	0.885	0.456
-1.0	0.707	0.556	0.783

Once the value of "a" and of α has been determined, the friction factor and the heat transfer coefficient are obtained directly as

$$C_{f_e} \sqrt{Re/2} = a \tag{64}$$

15

and

$$St \sqrt{Re_x} = \frac{w \ C_p \ \sqrt{Re_x} \ (\alpha - g_c)}{(1 - \alpha)} \tag{65}$$

NUMERICAL COMPUTATIONS

Equations (58) and (59) are first order differential equations and can be solved by any well known integration technique. Both equations involve the unknowns "a" and α and hence have to be solved simultaneously.

The continuous blowing at the wall gives rise to continuous boundary conditions. These equations therefore are very easily solved on CSMP (Continuous Systems Modeling Program). Numerical answers are obtained using fourth order Runge-Kutta, fixed-step integration technique. The step size used was $\Delta\xi = 0.0001$. To test the stability, this solution was compared with the answers obtained using rectangular Simpson's and Adam's method of integration (all the above techniques are available on CSMP). The answers obtained by all these techniques were within 0.5%.

The starting values of "a", i.e., a_{in}, are those given in Table I. For the flow near the stagnation point, the "in" value of "a" could be that given in Table I or II depending on the mode of injection. Same is true for the initial value of α. For wedge flows, the solution is carried out up to x = 0.9 ft. or until the value of "a" dropped below 0.02. For the 4:1 elliptic cylinder, the solution is obtained only over the front half while for the experimental airfoil, the solution covers the entire surface, suction and pressure. Any time the solution gave the value of "a" below 0.02, the computations were stopped. At this low value of the shear stress parameter the boundary layer is very thick and unstable and the prandtl boundary layer assumptions are no longer valid.

The numerical calculations were carried out for the following values of the variables:

Table III

Variable	Values	Flow Type
λ	-0.1, -0.2	
w	0.005, 0.01, 0.02, 0.05	
$\bar{U}_o$	200 ft/sec	
$\bar{T}_o$	2460 °R	Wedge Flow
$\bar{T}_c$	530 °R	
Re_o	10^5/ft	
λ	-1.0 to 0.0	
w	0.001, 0.005	
$\bar{U}_o$	800 ft/sec	Flow Over a 4:1
$\bar{T}_o$	2450 °R	(Major Axis: Minor Axis) Elliptic
$\bar{T}_c$	530 °R	Cylinder
Re_o	10^5 (based on half the major axis)	
λ	-1.0 to 0.023	
w	0.001, 0.002	
$\bar{U}_o$	142.8 ft/sec	Flow Over
$\bar{T}_o$	2460 °R	Airfoil
$\bar{T}_c$	530 °R	
Re_o	625000 (based on chord length)	

RESULTS AND DISCUSSION

To suppliment the present analysis, the answers obtained from Equations (58) and (59) are compared with the numerical computer solution of Equations (19) and (20). This program was developed by Davis and Werle[12]. The program is extremely versatile and gives solutions for:

1. Any Mach number, i.e., subsonic or supersonic;

2. Any Prandtl number; and

3. Any pressure gradient.

The program uses a much more realistic viscosity - temperature relationship given by Sutherland formula, than the linear relationship used in the analytical solution. It can be shown (see "Proposals for Further Research")[7] that if the more realistic $\mu \propto T^{0.75}$ relationship between viscosity and temperature is used, the solution of the momentum and energy equations would be slightly different.

Since "a" is a strong function of viscosity, the differences between the values of "a" obtained from the analytical solution and those obtained from the numerical solution (computer program) are likely to be more severe than the differences between the two values of the wall temperature. Also in the computation of Stanton number, due to the presence of the factor $(1 - \alpha)$ in the denominator, the differences between the two values of Stanton number are magnified.

Flow Over Wedges

The effects of uniform blowing on the wall temperature, local heat transfer (in the form of Stanton number) and local shear stress parameter for flow over wedges are shown in Figures 2 thorugh 7 (Figure 8 shows the velocity distribution over these wedges). Solutions are presented for ten-fold variation in the injection rate from $w = 0.005$ to $w = 0.05$. As to be expected, as the coolant injection rate increases, the wall temperature and the shear stress at the wall both decrease. With i.creasing distance from the leading edge, the wall temperature approaches coolant temperature $(\bar{T}_c)$ and the sheai stress approaches zero (blown-off boundary layer). At the leading edge, the temperature gradient is infinite (see Figures 2 and 5). This is due to the fact that in the present analysis the thermal conductivity of the wall has been neglected.

Comparison between the analytical values and numberical computer values of the wall temperatures is very good. For shear stress parameter, the numerical solution predicts a much steeper gradient than the analytical solution (for small values of x) and a more gentle one for large values of x. Agreement improves as the injection rate increases.

Flow at the Stagnation Point and Over the Surface of a Two-Dimensional Body in Crossflow

Effect of coolant injection through a porous wall of 4:1 (ratio of major axis to minor axis) elliptic cylinder is shown in Figures 9, 10 and 11. The velocity distribution and the pressure gradient parameter λ over this cylinder are given in Figure 12. This figure also shows the contour of the elliptic cylinder. The geometric parameters of the cylinder are

$$\varepsilon = 1 - [\frac{\text{Minor axis}}{\text{Major axis}}]^2 \qquad (66)$$

$$U_e = (1 + \Delta) \sin (\theta) / \sqrt{1 - \varepsilon \cos^2 (\theta)} \qquad (67)$$

where

$$\Delta = \frac{\text{Minor axis}}{\text{Major axis}} \qquad (68)$$

and θ is the angle measured in radians from the front stagnation point.

$$x = \int_0^\theta \sqrt{1 - \varepsilon \cos^2 (\theta)} \; d\theta \qquad (69)$$

These values were obtained from Evans[13] (the reference length is (Major axis)/2).

Agreement between the numerical and analytical values is very good. Analytical solution is presented with and without Euler transformation. As far as the wall temperature distribution is concerned, (Figure 9), the Euler transformation does not make much difference. However, for the shear stress parameter, the solution obtained with the Euler transformation agrees much better with the computer answers than that obtained without Euler transformation.

The agreement between the analytical and numerical solutions clearly support the validity of the assumptions made earlier. It was assumed that for small absolute values of $N (|N| < 0.7)$, terms involving higher powers of N (e.g., N^2, $(\xi \, dN/d\xi)^2$ etc.) could be neglected for the coefficients of η^5, η^6, η^7 and η^8. (In fact, for η^7 and η^8 all terms involving N are negligible.) Very good agreement between the numerical and analytical values shows that the contribution by these terms is indeed small enough to be neglected.

It is necessary to realize that this assumption is valid only (i) for small injection flow rates (which are likely to be encountered in the turbine blade cooling); and (ii) near the front

19

stagnation point.

Near the stagnation point, λ is of the order of -1.0 and N is at least one order of magnitude lesser. Consequently, the terms involving N^2, $[\xi(N)_\xi]^2$ etc. are very small. Away from the stagnation point (i.e., with increasing x), the absolute value of λ decreases while that of N increases. Downstream from the crossover point (this is the value of x when $|\lambda| = |N|$), the contribution of higher order N-terms becomes important. Fortunately for most any two-dimensional body in crossflow for small injection rates, this crossover point will occur far enough downstream from the stagnation point such that the contribution by the n^5 or higher terms (of the series) will be small enough to be neglected. Hence, the validity of the assumptions will hold for all values of x.

As mentioned in the chapter on the stagnation point solution, the initial conditions for the stagnation flow depend on the mode of injection. If the injection starts for $x > 0$, the initial values are:

$$a_{in} = 1.234 \qquad \text{(with Euler transformation)}$$

$$\alpha_{in} = 1.0$$

If, however, the injection is assumed to initiate from $x = 0$, the initial conditions are the values given in Table II. These values are also presented in Figures 13 and 14. Figure 13 also shows the stagnation point temperature obtained by other investigators. The present analysis predicts slightly lower values of the stagnation point temperature throughout the range of injection considered ($w = 0.001$ to $2 = 0.01$). The solution is valid for any two-dimensional body in crossflow provided the value of N at the stagnation point does not exceed (in the negative sense) -1.0.

Solutions of the wall temperature and the shear stress for the 4:1 elliptic cylinder with the initial values obtained from Table II (i.e., stagnation values) are also presented in Figures 9 and 11. In all cases, the solutions quickly merge with the one obtained with the initial values from Table I.

Flow Over an Airfoil

The stagnation point analysis is also applied to the flow over an airfoil (shown in Figure 15). The experimental velocity distribution over the airfoil was obtained by M. Hussein and W. Tabakoff[14]. Readings were taken at the room temperature, with $U_O = 142.6$ ft/sec and Reynolds number (based on chord length) = 625,000. The values of λ and $d\lambda/d\xi$ were calculated from Figure 16 (which gives the velocity distribution over the suction and the pressure side of the airfoil).

Figures 17 through 22 show the wall temperature distribution, heat transfer and the friction factor (instead of shear stress parameter) over the suction side and pressure side of the airfoil for w = 0.001 and w = 0.002. As before, blowing is very effective in lowering the airfoil surface temperature but at the same time it induces instability which may result either in transition to turbulence or laminar blow-off.

Effect of Inclusion of Higher Order Terms in η on the Flat Plate and Wedge Flows

To find the effect of inclusion of higher order terms, i.e., Equations (58) and (59) on flat plate (Reference 1) and wedge flows, these equations (Equations (58) and (59)) are again solved for $\lambda = 0$, $\lambda = -0.1$ and $\lambda = -0.2$. Other parameters are the same as those given in Table III. Solutions with and without Euler transformation are presented for w = 0.01 in Figures 23 through 25. Surprisingly, the assumptions made in derivation of Equation (58) and Equation (59) are more critical for wedge flows.

For values of λ of the order of $\lambda = 0$ to $\lambda = -0.1$, the contribution due to the terms η^5 or higher in the series expansions is quite small. The assumptions then are not critical. The solutions (with as well as without Euler transformation) show that as the number of terms in the series are increased, the agreement between numerical and the analytical results improve. The two solutions agree very well.

As the absolute value of λ increases, i.e., $\lambda = -0.2$ say, the contribution by the higher order terms in the series becomes important. For the wedge flows λ is constant, independent of the downstream distance. Even for small values of x, the value of N here is comparible to that of λ. Here the crossover point occurs much nearer the leading edge than in the case of a two-dimensional body in crossflow. Consequently, results of Equations (58) and (59) show larger deviation from the numerical values for $\lambda = -0.2$.

For the flat plate and wedge flow solutions also the results with Euler transformation are slightly better than those without Euler transformation. For the flat plate, the values of the wall temperature and the shear stress obtained with or without the transformation are so close that within the scale of the graph, they could hardly be differentiated.

Boundary Layer Blow-Off

As mentioned before, when the shear stress parameter drops to a very low value (below 0.02) the boundary layer becomes unstable. In the present analysis, the solution of the equations is terminated when the value of "a" reaches very low values (0.02 to 0.01). The

present theory does not give satisfactory answer as to whether the laminar boundary layer will undergo transition to turbulent boundary layer or will get blown off when shear drops to very low values. A more thorough investigation is necessary to evaluate the effect of injection on laminar boundary layer stability.

CONCLUSIONS

An analytical solution for compressible laminar boundary layer with continuous mass injection was derived. Here the previous work[1] is extended such that the solution is valid for any pressure gradient including the stagnation point; for subsonic flows with a Prandtl number of one and for a linear viscosity-temperature relationship. The method, however, can be broadened to consider high Mach numbers and real representation of Prandtl number and viscosity temperature variation. Numerical examples for the wall temperature and shear stress were obtained for continuous injection and the values compared with exact computer solutions. Very good agreement between the two values of wall temperature was realized. The agreement in the shear stress values is fair.

The following general conclusions are drawn:

(i) For transpiration cooling, the wall temperature falls rapidly with increasing injection mass flow rate and the temperature gradient is infinite at the leading edge.

(ii) Injection of the coolant into the boundary layer makes the layer unstable. This is most likely to cause early transition from laminar to turbulent boundary layer.

(iii) When the shear stress parameter "a" drops below 0.02, the solution becomes unstable.

(iv) In cooling a turbine blade by transpiration cooling method, an injection rate of 0.5% of the main flow is sufficient to maintain the blade temperature below 65% of the mainstream temperature.

(v) Injection of mass into the laminar boundary layer causes instabilities in the boundary layer and may result either in transition to turbulent boundary layer or laminar blow-off. Further investigation is necessary to study these phenomena.

22

REFERENCES

1. Pavri, R. and Tabakoff, W., "An Analytical Solution of Wall Temperature Distribution for Transpiration and Local Mass Injection Over a Flat Plate," AIChE - ASME Heat Transfer Conference, Denver, Colorado, Paper No 72-HT-57.

2. Gollnick, Jr., A.F., "Thermal Effects on a Transpiration Cooled Hemisphere," J. Aero. Sci., 29, 583-590, 595, 1962.

3. Goodwin, G. and Howe, J.T., "Recent Developments in Mass, Momentum, and Energy Transfer at Hyper Velocities," NASA SP-24, 1962.

4. Bayley, F.J. and Turner, A.B., "The Transpiration Cooled Gas Turbine," ASME Paper No. 70-GT-56, 1970.

5. Nealy, D.A. and McFadden, P.W., "Some Boundary Layer Porous Wall Coupling Effects in Laminar Flows with Surface Injection," ASME Paper No. 70-GT-1, 1970.

6. Morduchow, M., "On Heat Transfer Over Sweat-Cooled Surface in Laminar Compressible Flow with Pressure Gradient," J. Aero. Sci., 19, 705-712, 1952.

7. Pavri, R.E., Ph.D. Thesis, Department of Aerospace Engineering, University of Cincinnati, 1972.

8. Meksyn, D., "New Methods in Laminar Boundary Layer Theory," Pergamon Press, 1961.

9. Bromwich, T.A. and Macrobert, T.M., "An Introduction to the Theory of Infinite Series," University Press, London, 1949.

10. Hardy, G.H., "Divergent Series," Clarendon Press, Oxford, 1949.

11. Knopp, K., "Theory and Application of Infinite Series," 2nd ed., Blackie Press, 1951.

12. Davis, R.T. and Werle, M.J., "Private Communication," Department of Aerospace Engineering, University of Cincinnati.

13. Evans, H.L., "Laminar Boundary Layer Theory," Addison Wesley Co., 1968.

14. Hussein, M.F. and Tabakoff, W., "The Properties of a Gas Particle Flow in Cascade," U.S. Government Research and Development Report AD-697164, September, 1969.

15. Sparrow, E.M., Torrance, K.E. and Jung, L.Y., "Flow and Heat Transfer," Proceedings of the Third International Heat Transfer Converence, August, 1966.

TABLE IV

Explanation Of Symbols Used In The Figures

Symbol	w	Remarks
$\lozenge$, $\bigcirc$	0.001	Each symbol in the figure
$\bigcirc$	0.002	represents a data point obtain-
$\square$, $\sqsubset$	0.005	ed from the numerical computer
$\diamondsuit$	0.01	solution.
$\triangle$	0.02	
$\triangleright$	0.05	

——— (Except in Figs. 9-22)	Integral solution, terms up to η^3 in the series.
- - - - - (Except in Figs. 9-22)	Integral solution, terms up to η^8 in the series (with Euler Transformation).
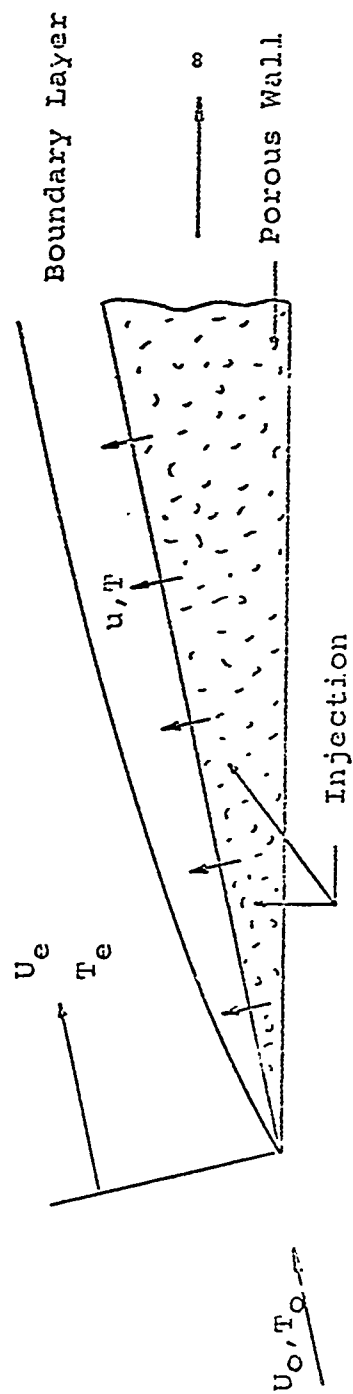
FIGURE 1   PHYSCIAL MODEL FOR FLOW OVER A WEDGE
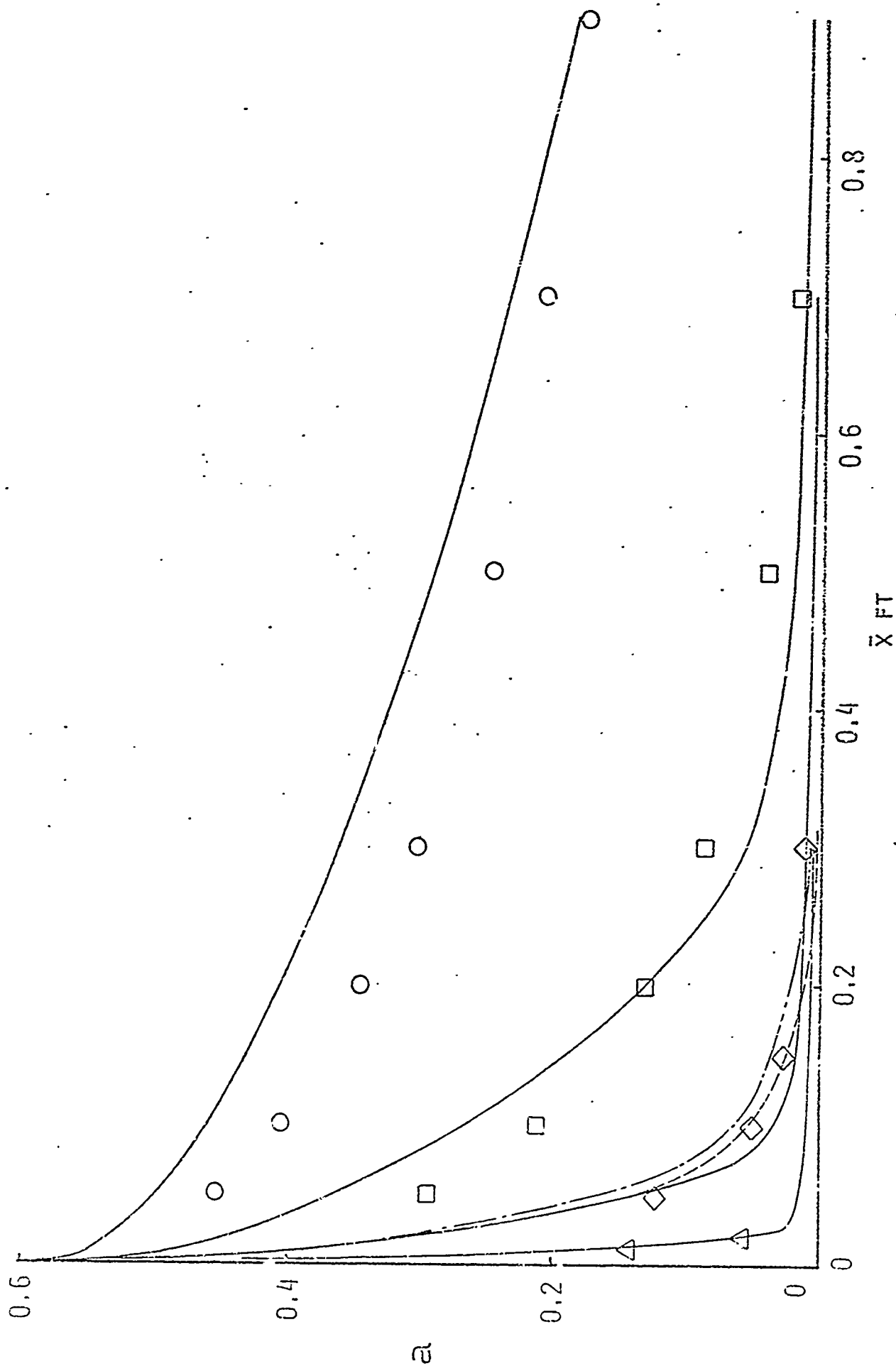
FIGURE 2   LOCAL VALUES OF THE SHEAR STRESS PARAMETER FOR THE TRANSPRIATION COOLED WALL
$\lambda = -0.1$

26
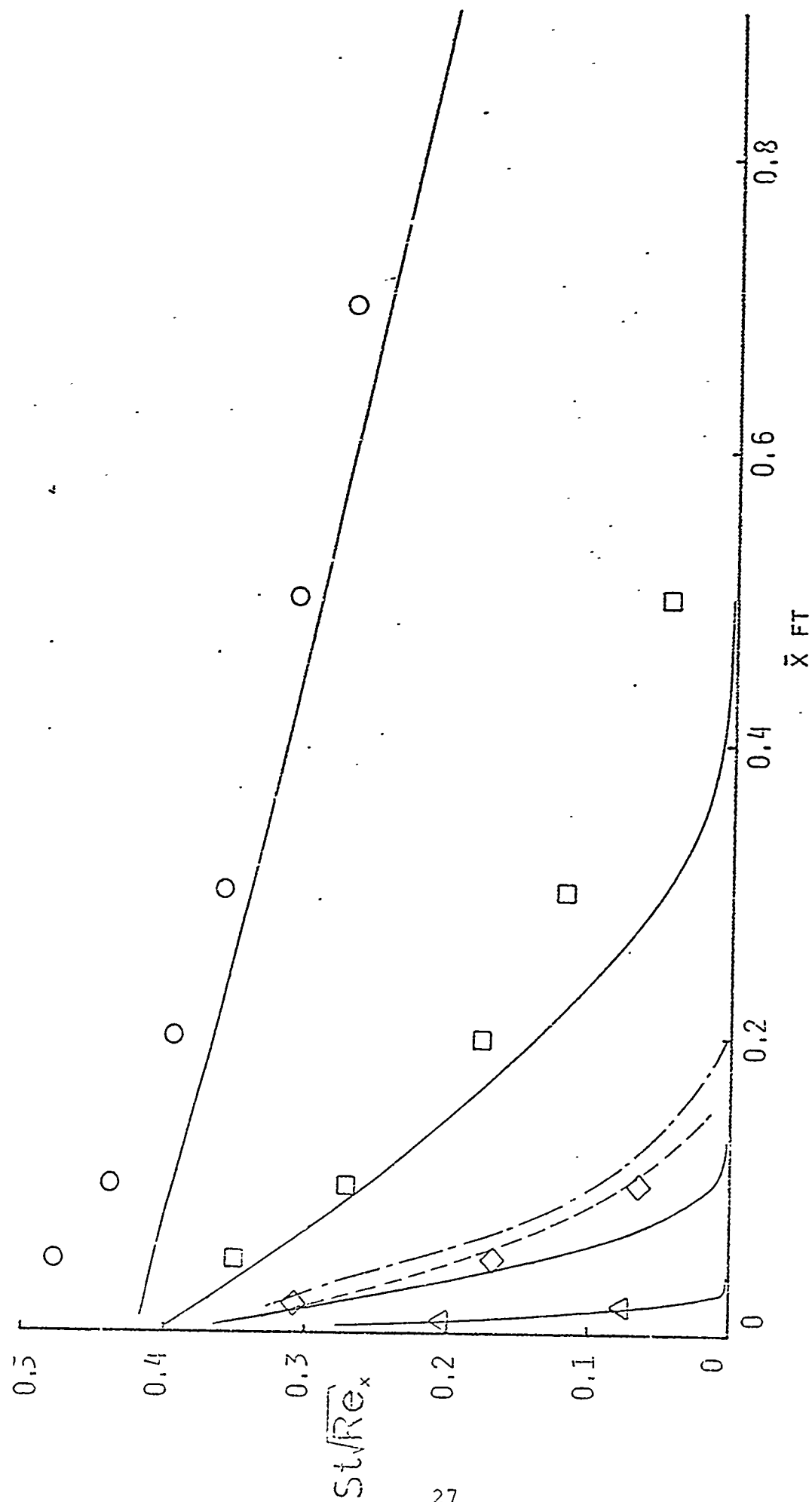
FIGURE 3   LOCAL VALUES OF STANTON NUMBER FOR THE TRANSPIRATION COOLED WALL, $\lambda = -0.1$.

27
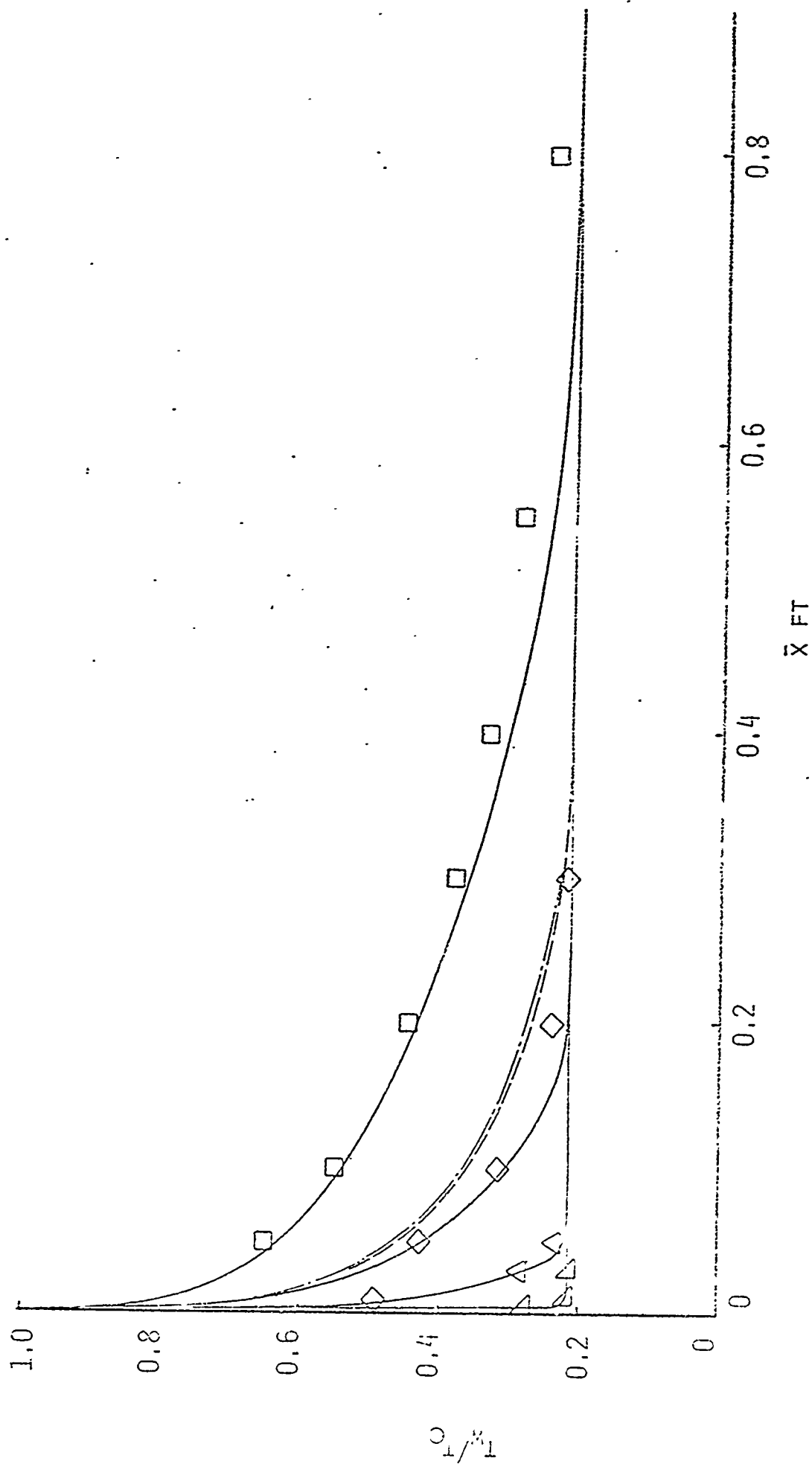
FIGURE 4   TRANSPIRATION COOLED WALL TEMPERATURE DISTRIBUTION, $\lambda = -0.2$
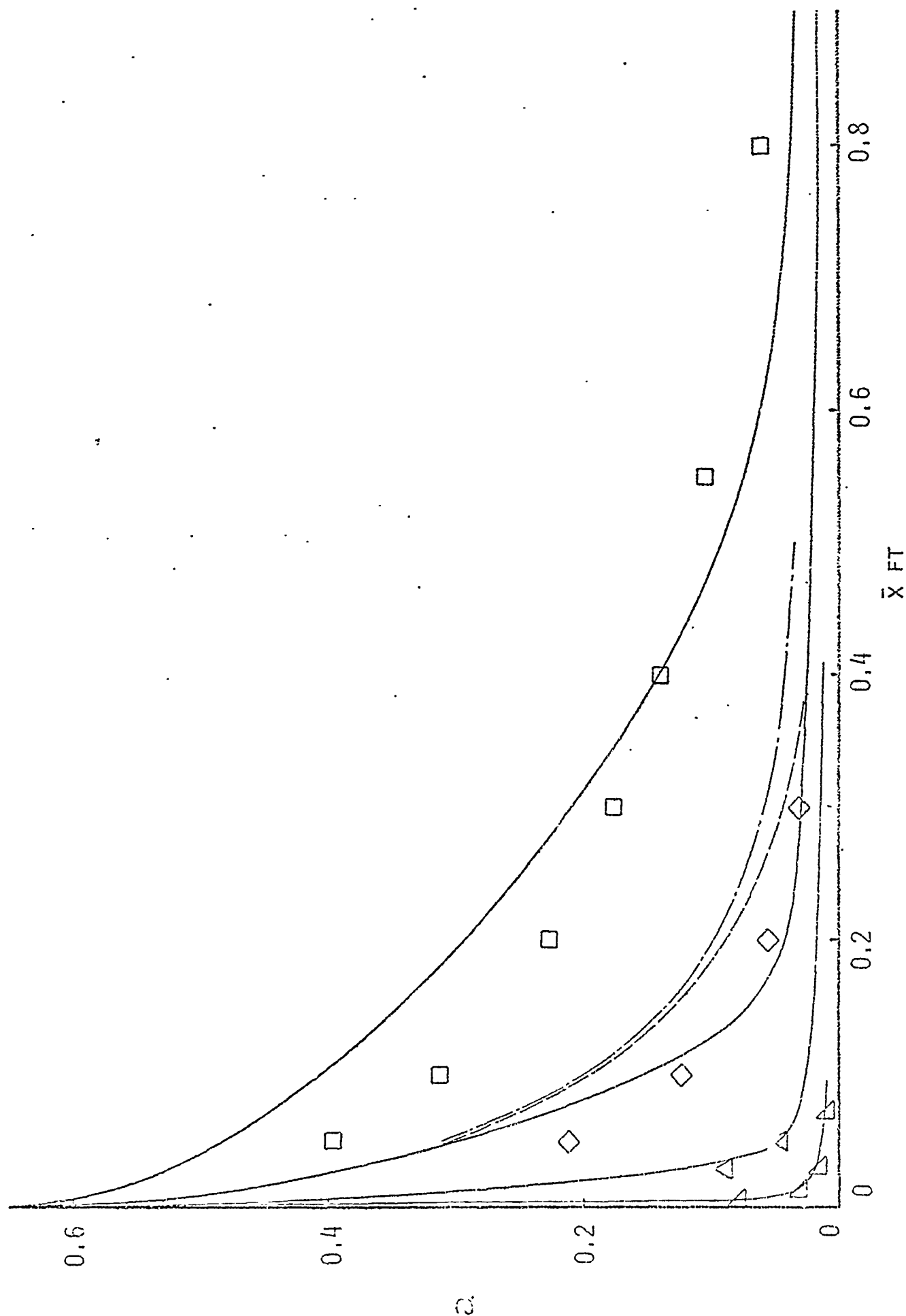
FIGURE 5   LOCAL VALUES OF THE SHEAR STRESS PARAMETER FOR THE TRANSPIRATION COOLED WALL, $\lambda = -0.2$

29
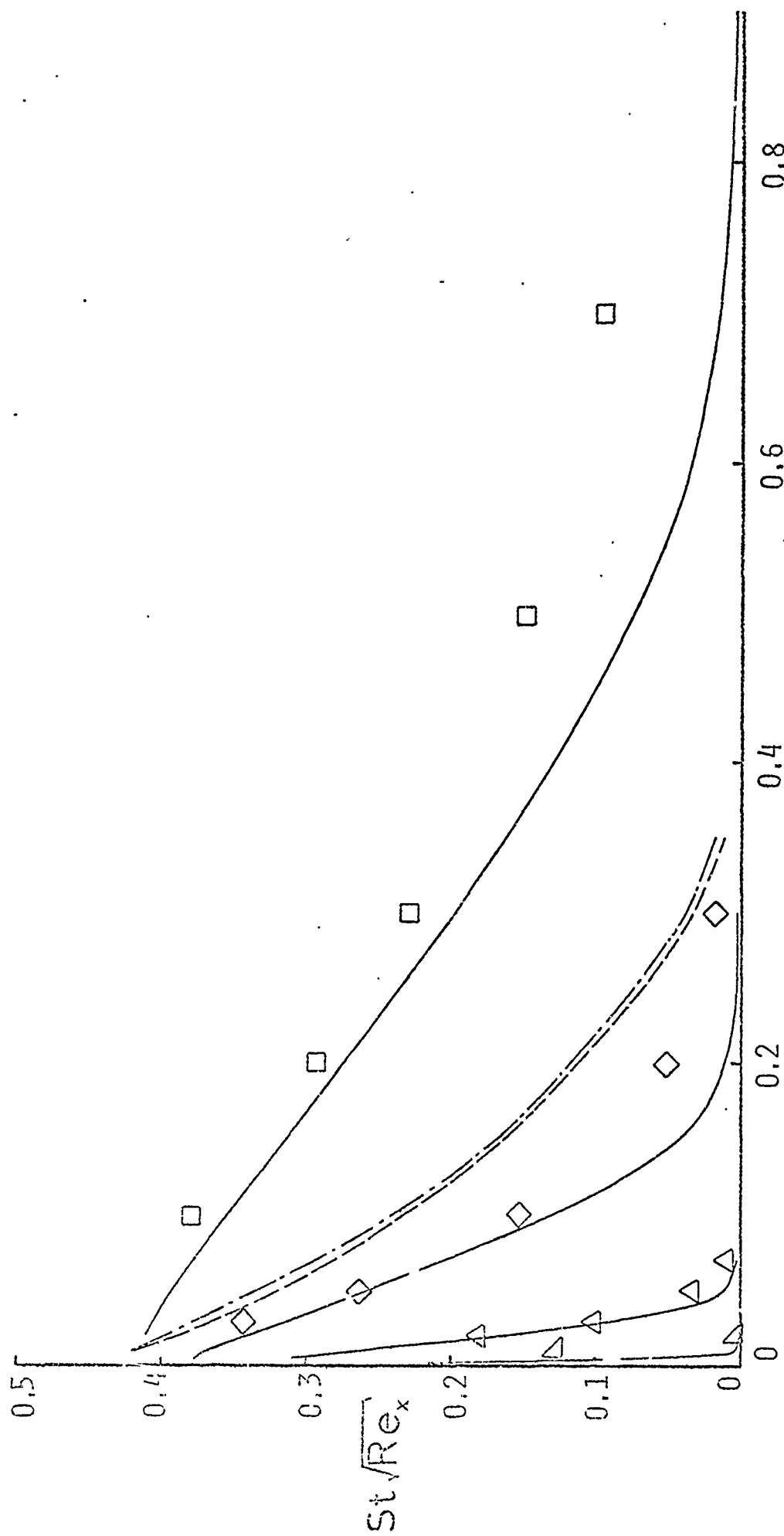
FIGURE 6   LOCAL VALUES OF STANTON NUMBER FOR THE TRANSPIRATION COOLED WALL, $\lambda = -0.2$
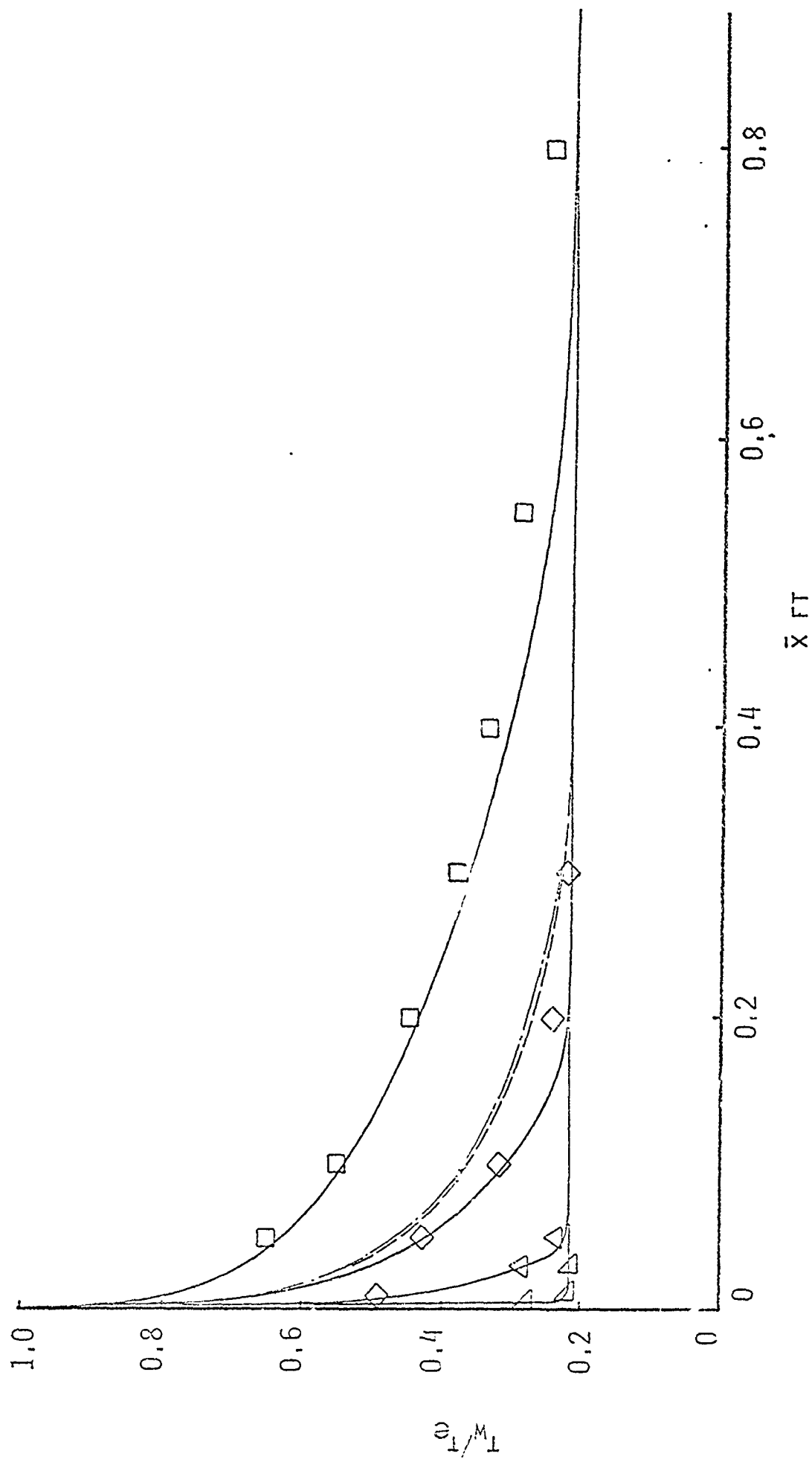
FIGURE 7   TRANSPIRATION COOLED WALL TEMPERATURE DISTRIBUTION, $\lambda = -0.2$
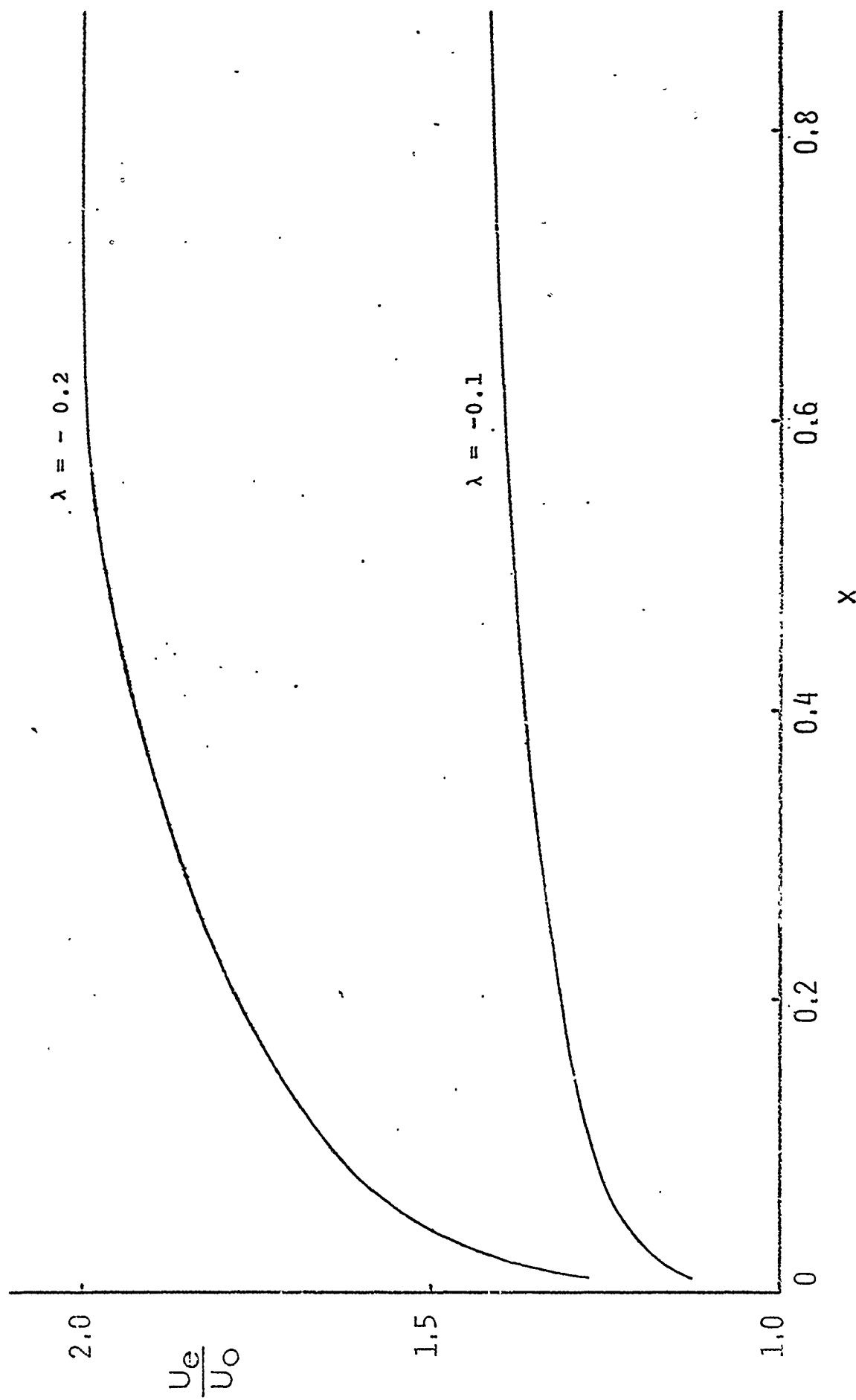
FIGURE 8 VELOCITY DISTRIBUTION OVER WEDGES

32
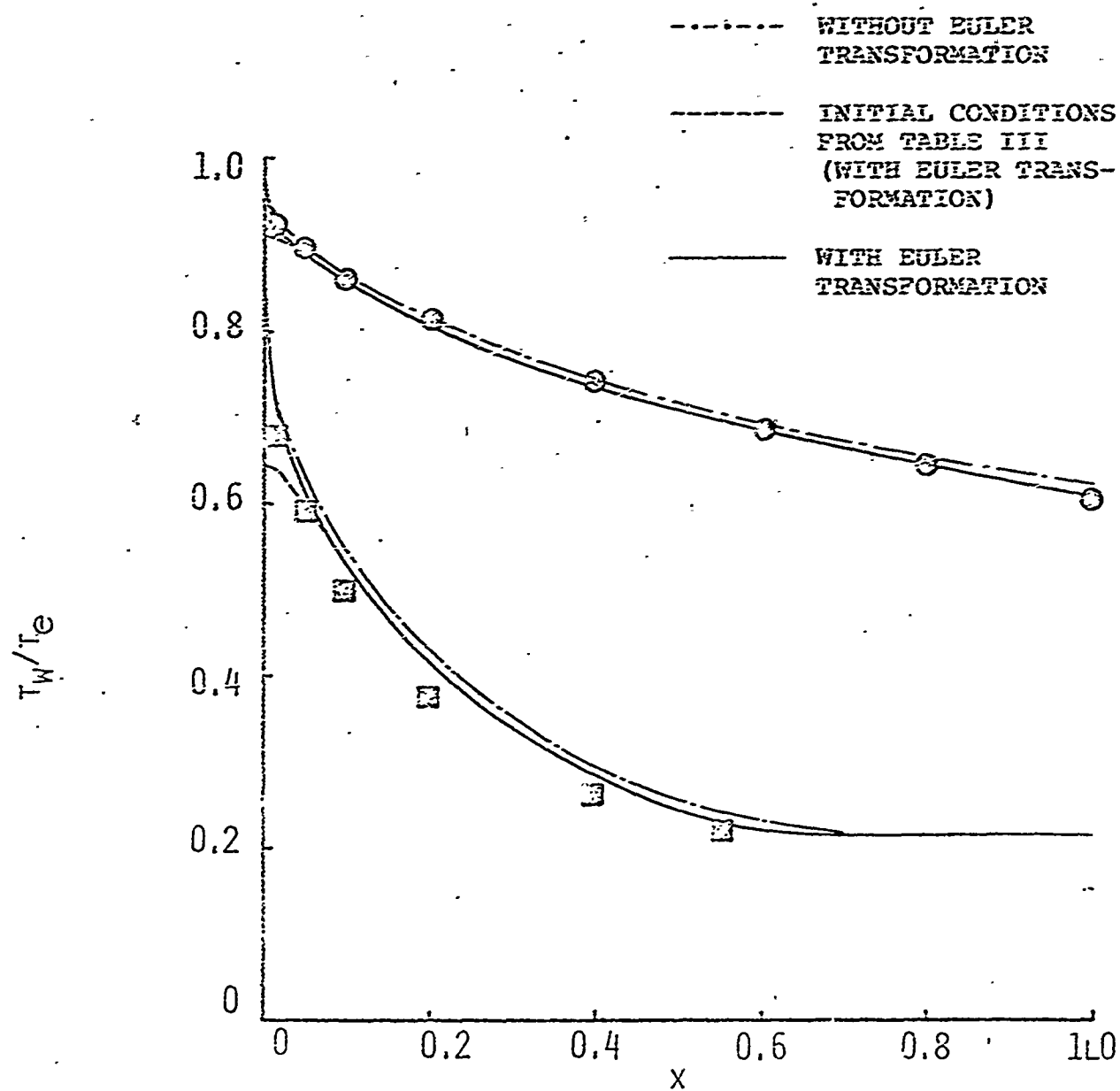
FIGURE 9   WALL TEMPERATURE DISTRIBUTION FOR THE 4:1 ELLIPTIC
CYLINDER

$St\sqrt{Re_x}$

WITHOUT EULER
TRANSFORMATION

WITH EULER
TRANSFORMATION
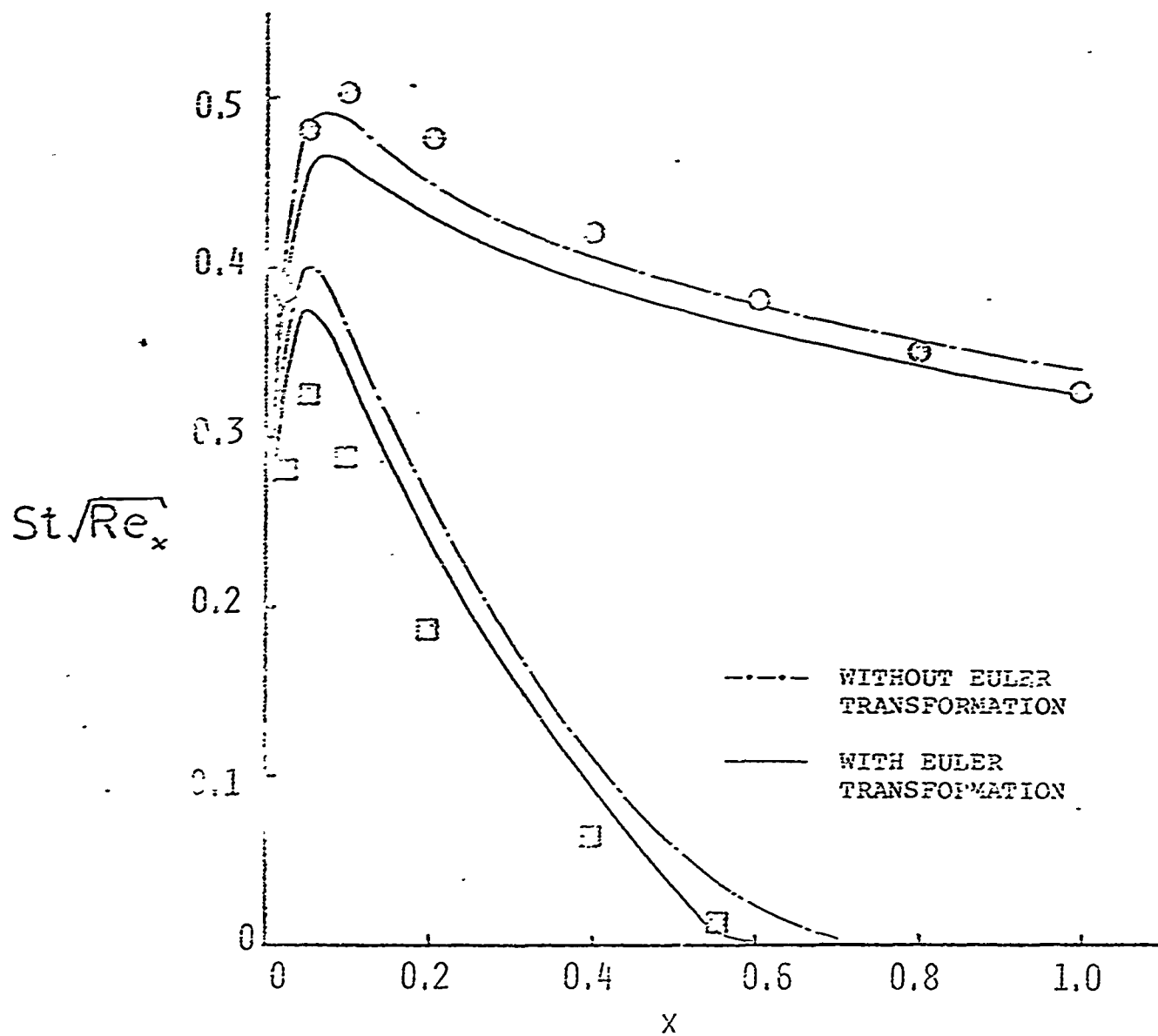
FIGURE 10   LOCAL VALUES OF HEAT TRANSFER ALONG THE SURFACE OF THE
4:1 ELLIPTIC CYLINDER
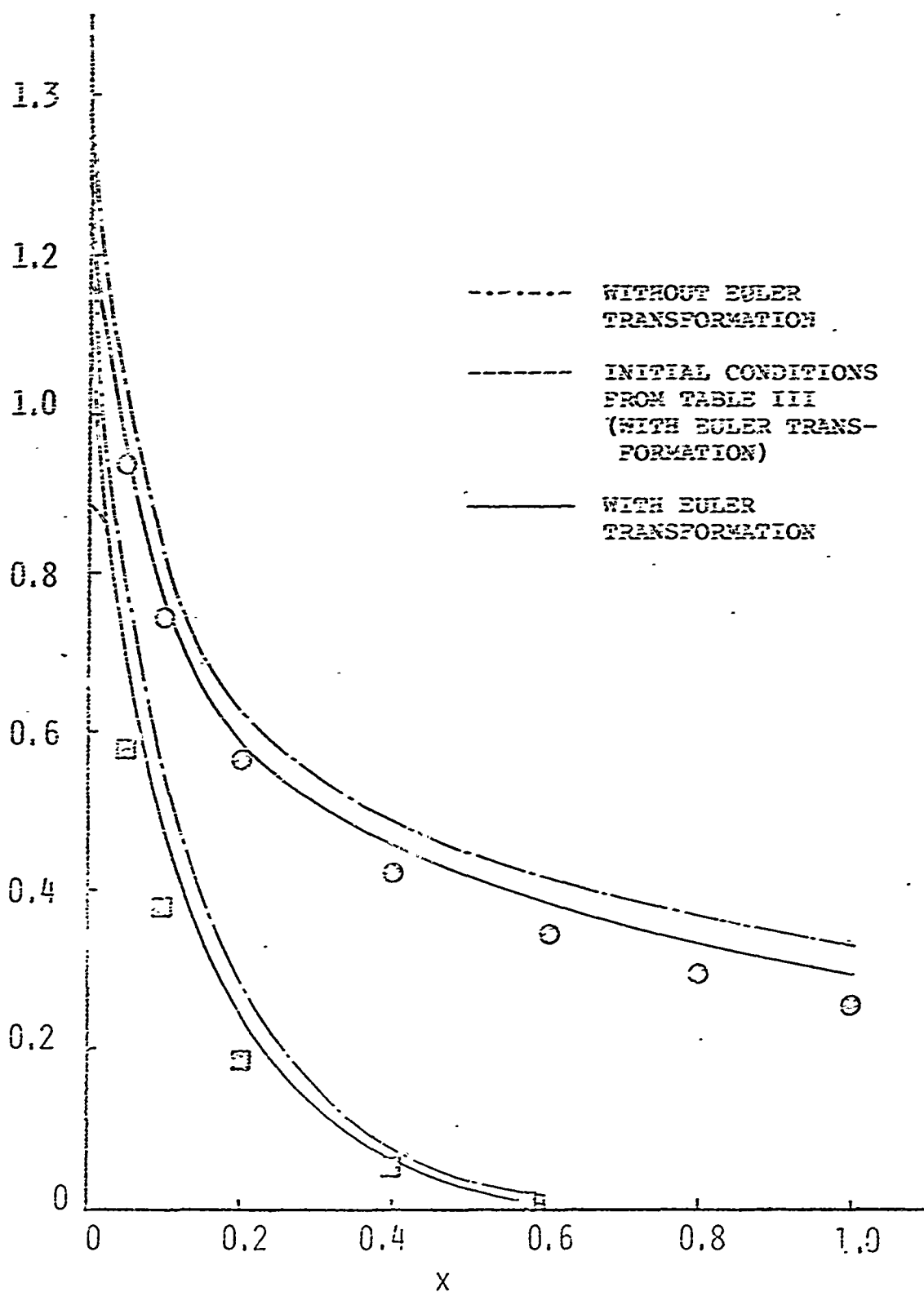
FIGURE 11   SHEAR STRESS PARAMETER FOR THE 4:1 ELLIPTIC CYLINDER
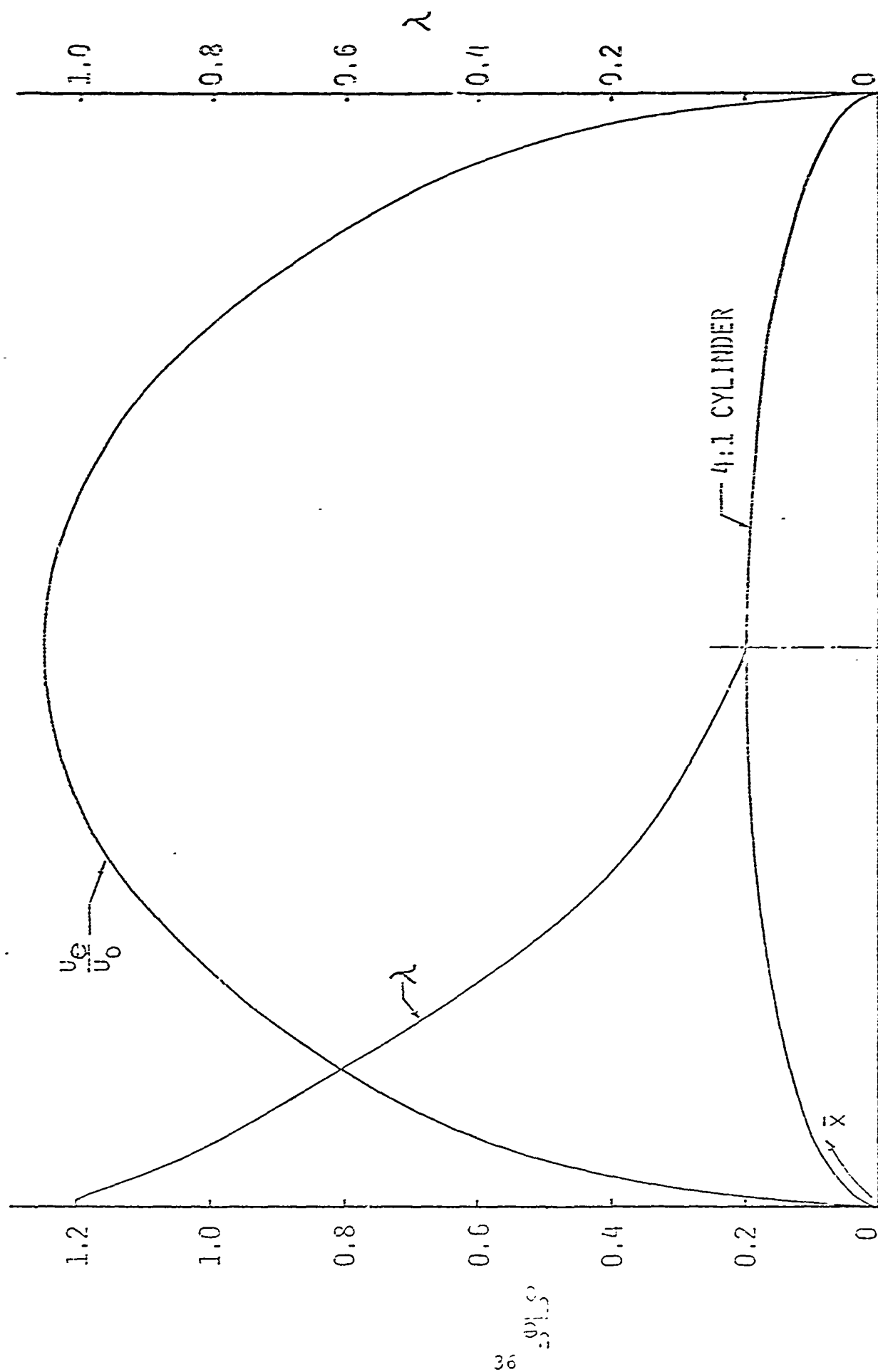
FIGURE 12 VELOCITY DISTRIBUTION ON A 4:1 ELLIPTIC CYLINDER

36
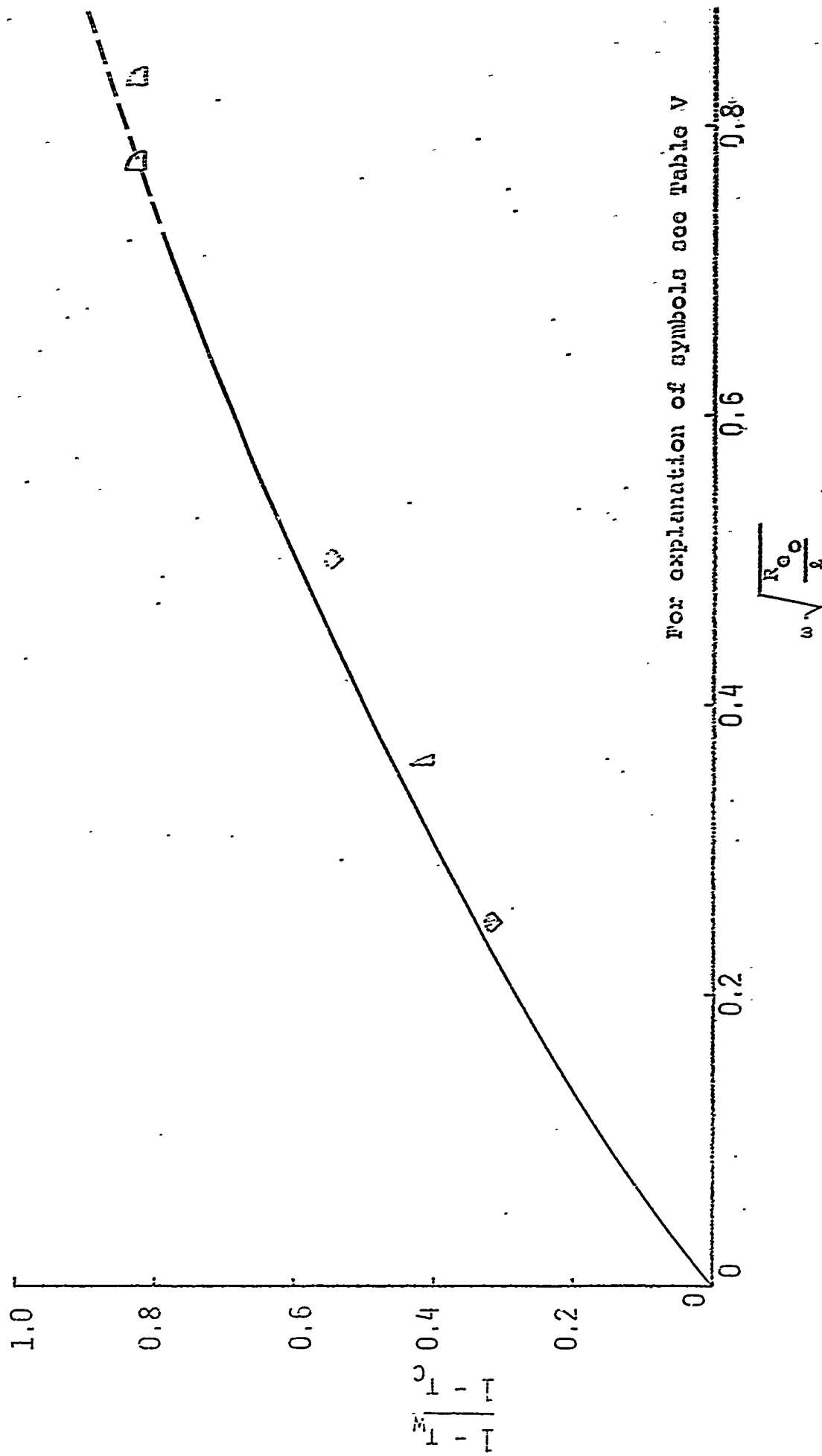
FIGURE 13   STAGNATION POINT TEMPERATURE FOR A TWO-DIMENSIONAL BODY IN CROSSFLOW WITH TRANSPIRATION COOLING

For explanation of symbols see Table V

$$\sqrt[3]{\frac{R_Q Q}{\ell}}$$

$$\frac{T - T_c}{T_w - T_c}$$

37

TABLE V

Nomenclature for Figure 13

Symbol	Reference	Remarks
◇	15	Cylinder in Crossflow; $U_e = 2 \sin(x)$
⚑	5	Two-Dimensional Body in Crossflow; $U_e = \sin(\pi x/2)$
⌂	6	Turbine Blade; Velocity Distribution obtained from a figure in the Reference
⌂	5	Same Turbine Blade; Computer Solution
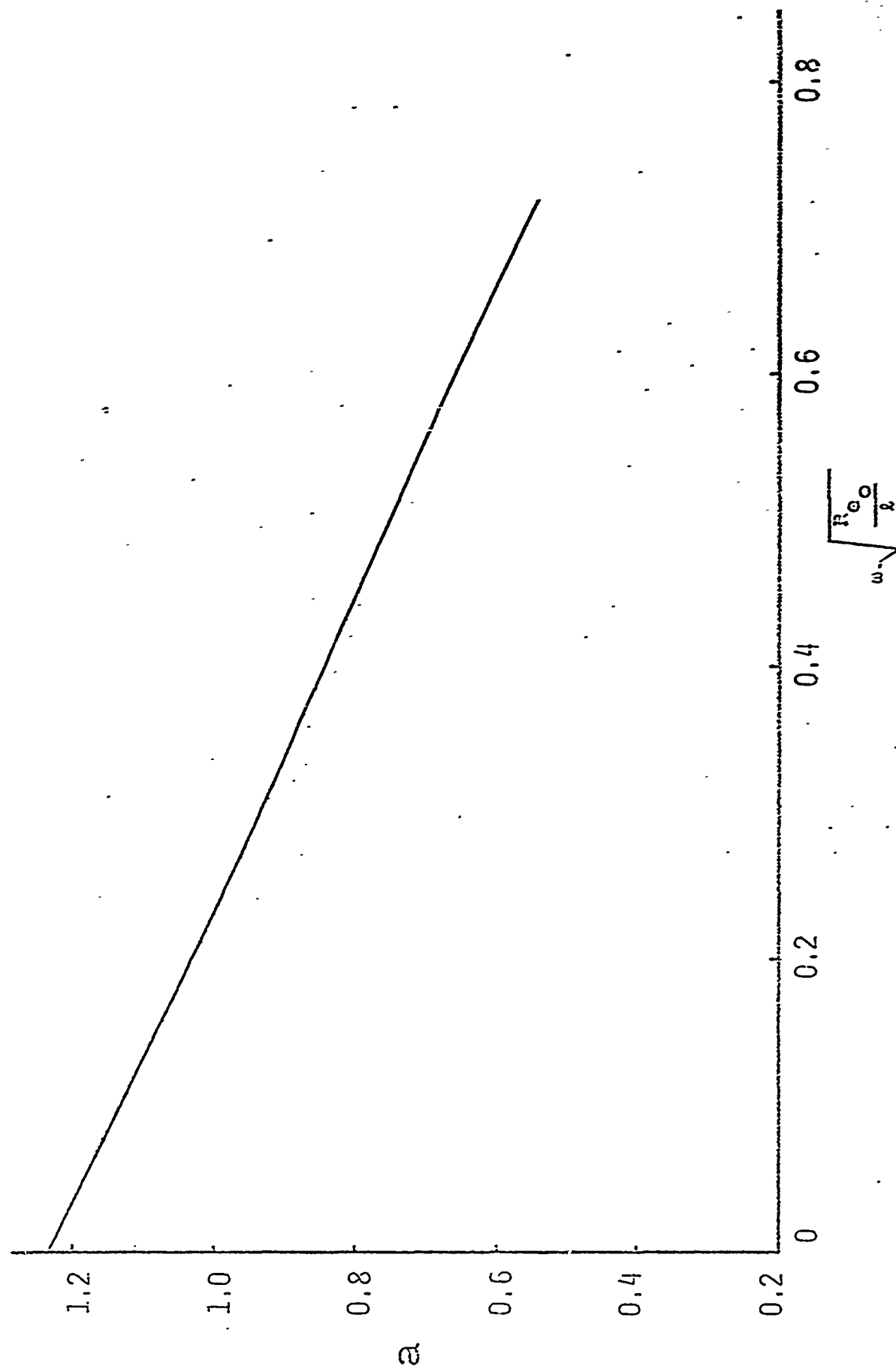
FIGURE 14   STAGNATION VALUES OF "a" FOR A TWO-DIMENSIONAL BODY IN CROSSFLOW WITH TRANSPIRATION COOLING
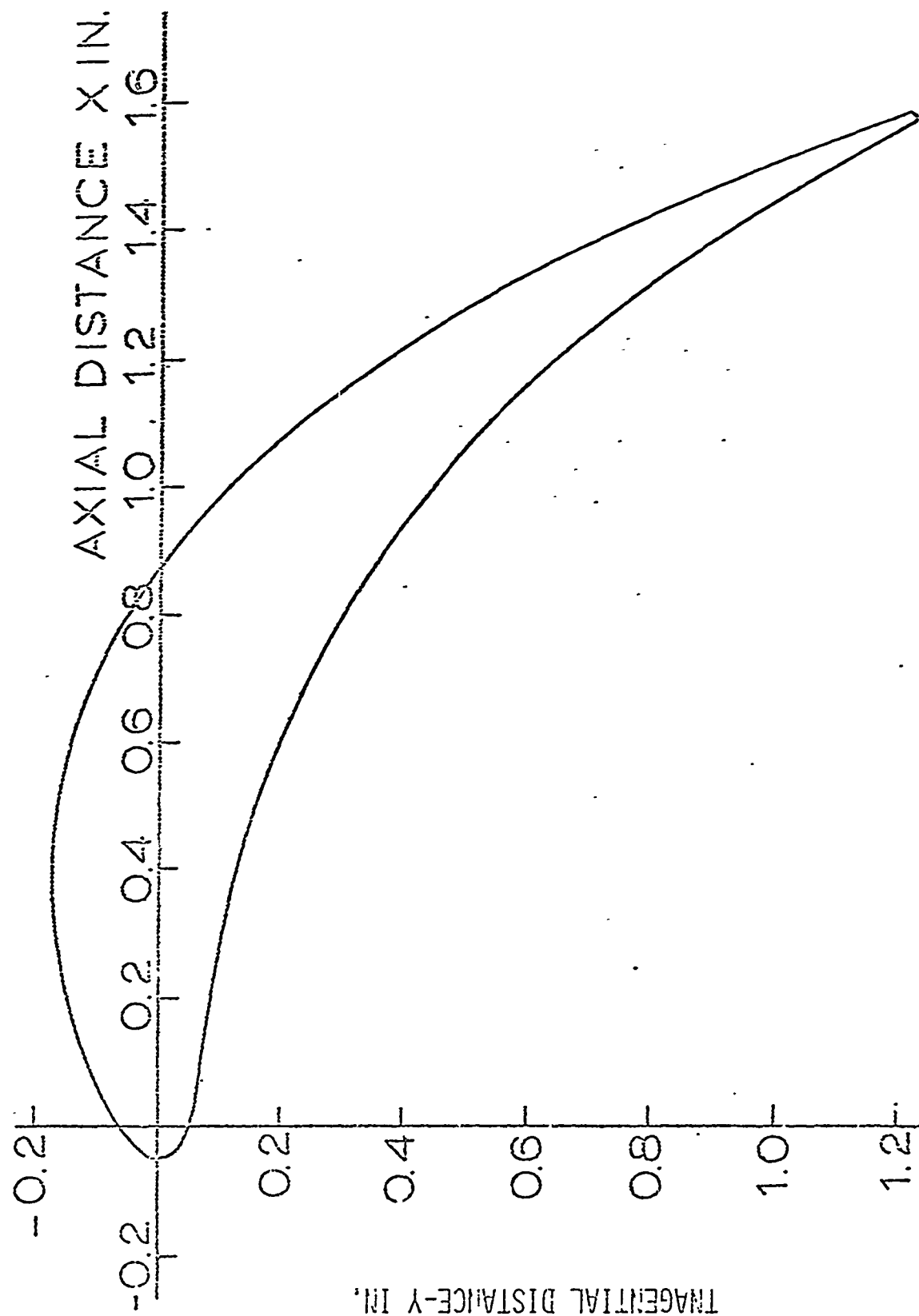
FIGURE 15   AIRFOIL SHAPE

40
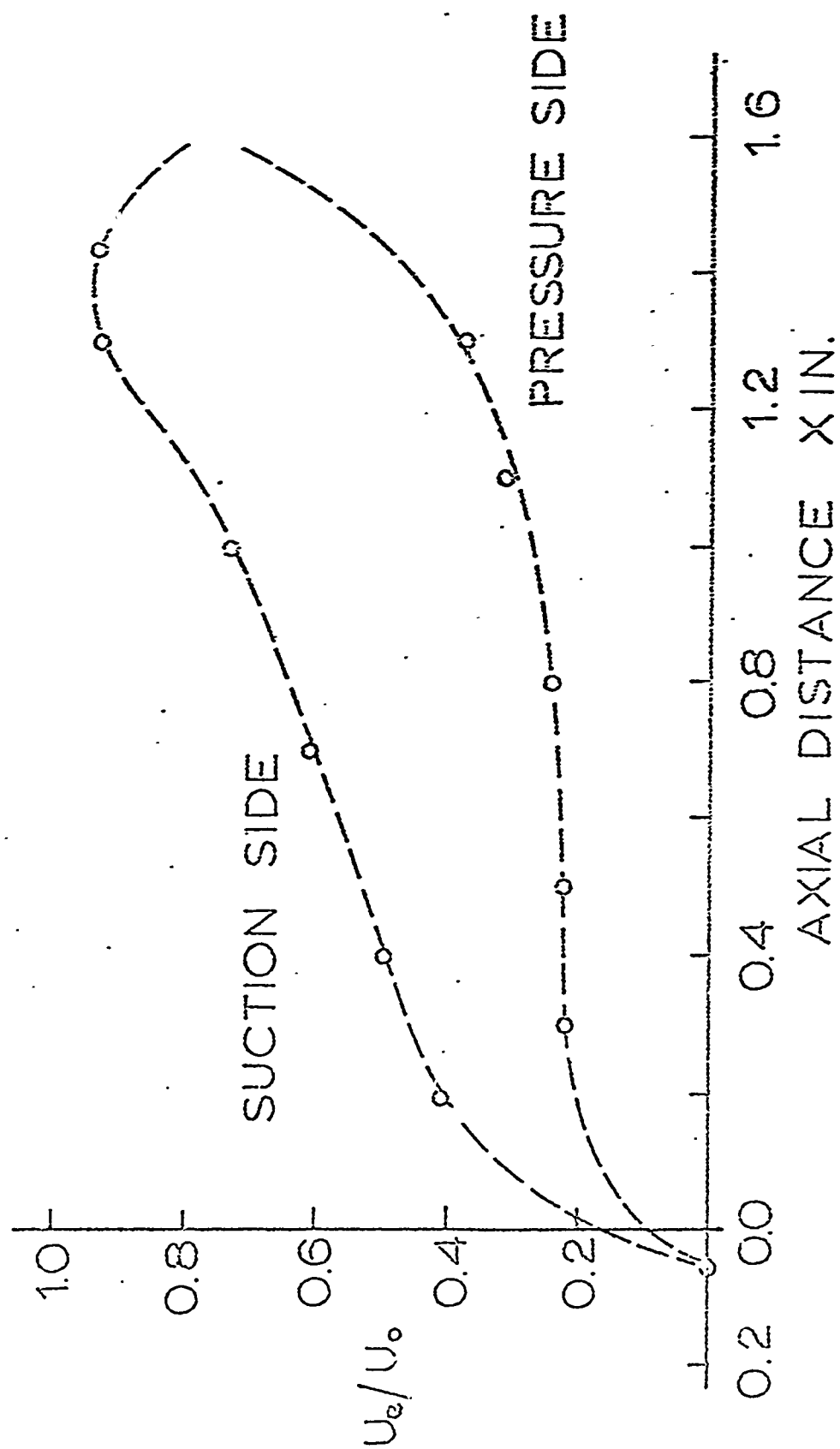
FIGURE 16 EXPERIMENTAL VELOCITY DISTRIBUTION OVER THE AIRFOIL.

41
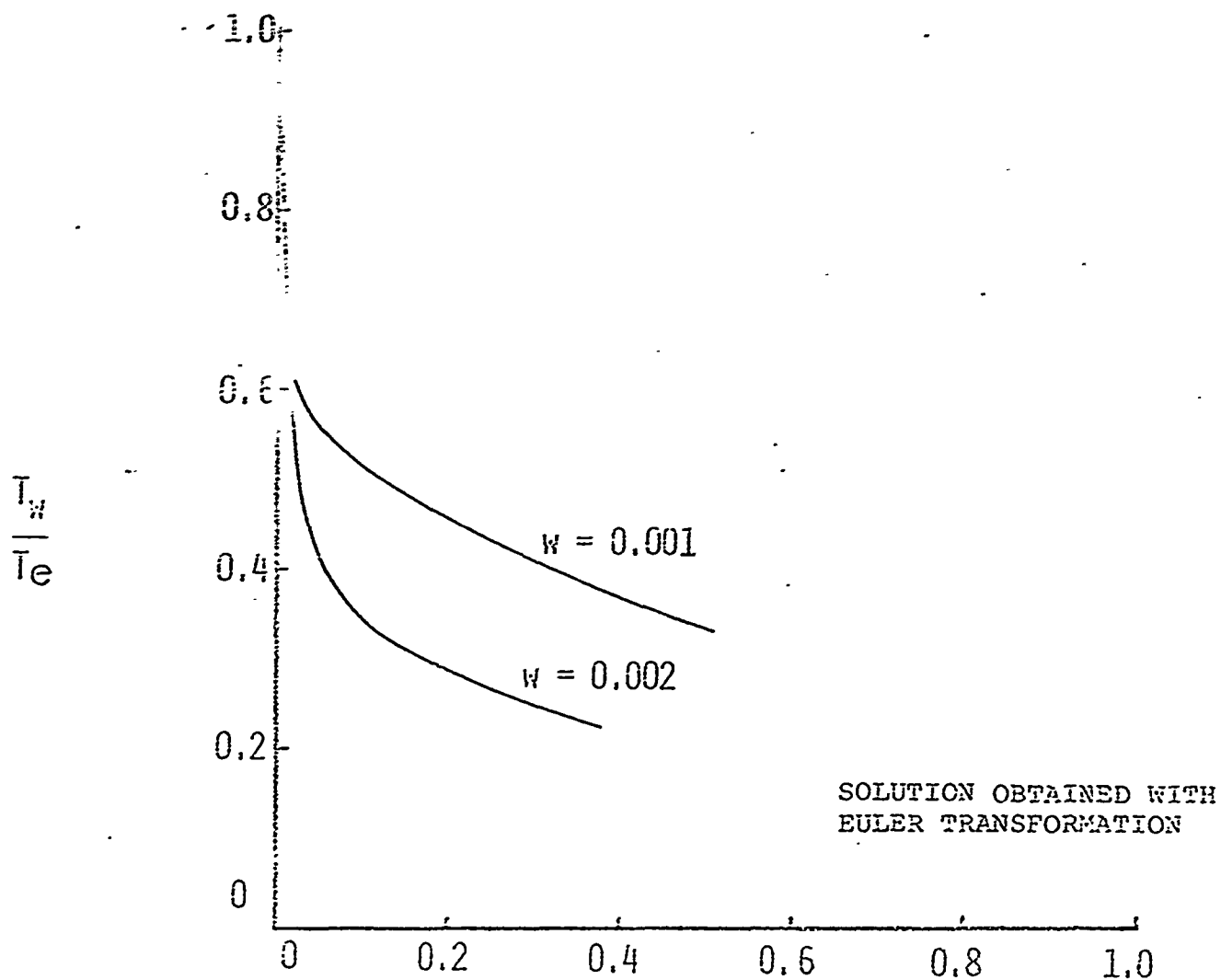
FIGURE 17 WALL TEMPERATURE DISTRIBUTION OVER THE SUCTION SIDE OF
THE AIRFOIL
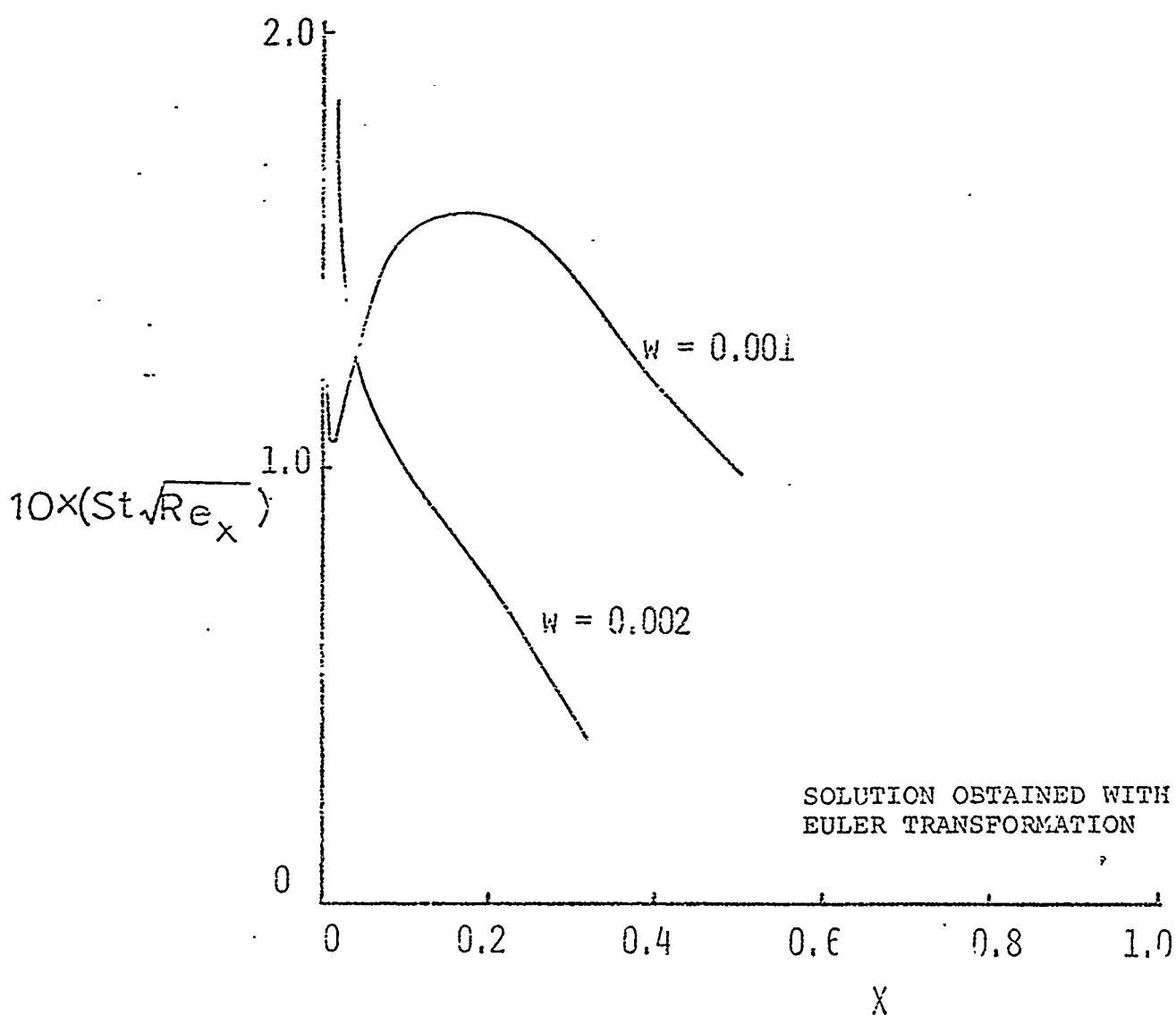
FIGURE 18 HEAT TRANSFER OVER THE SUCTION SIDE OF THE AIRFOIL

43
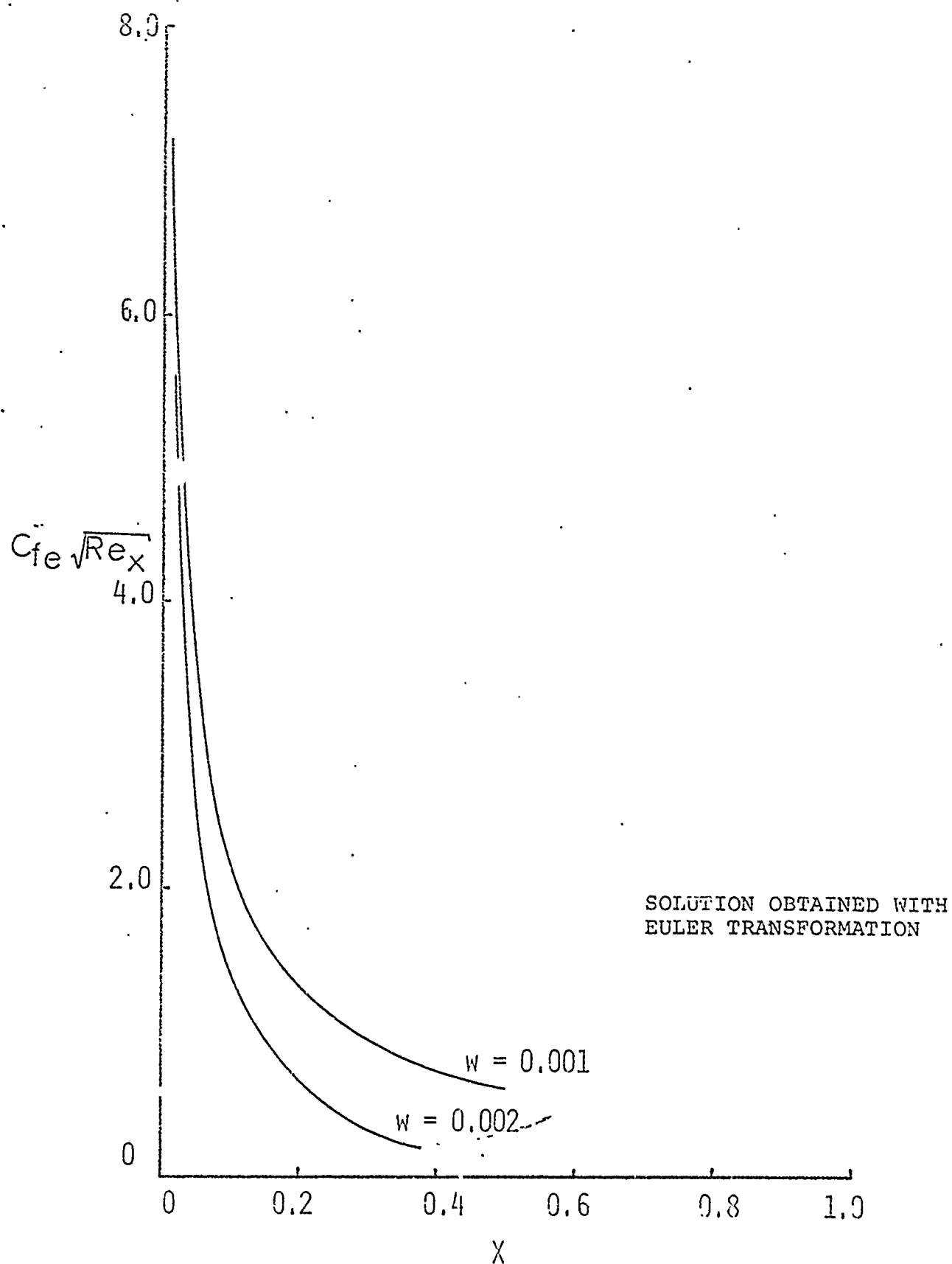
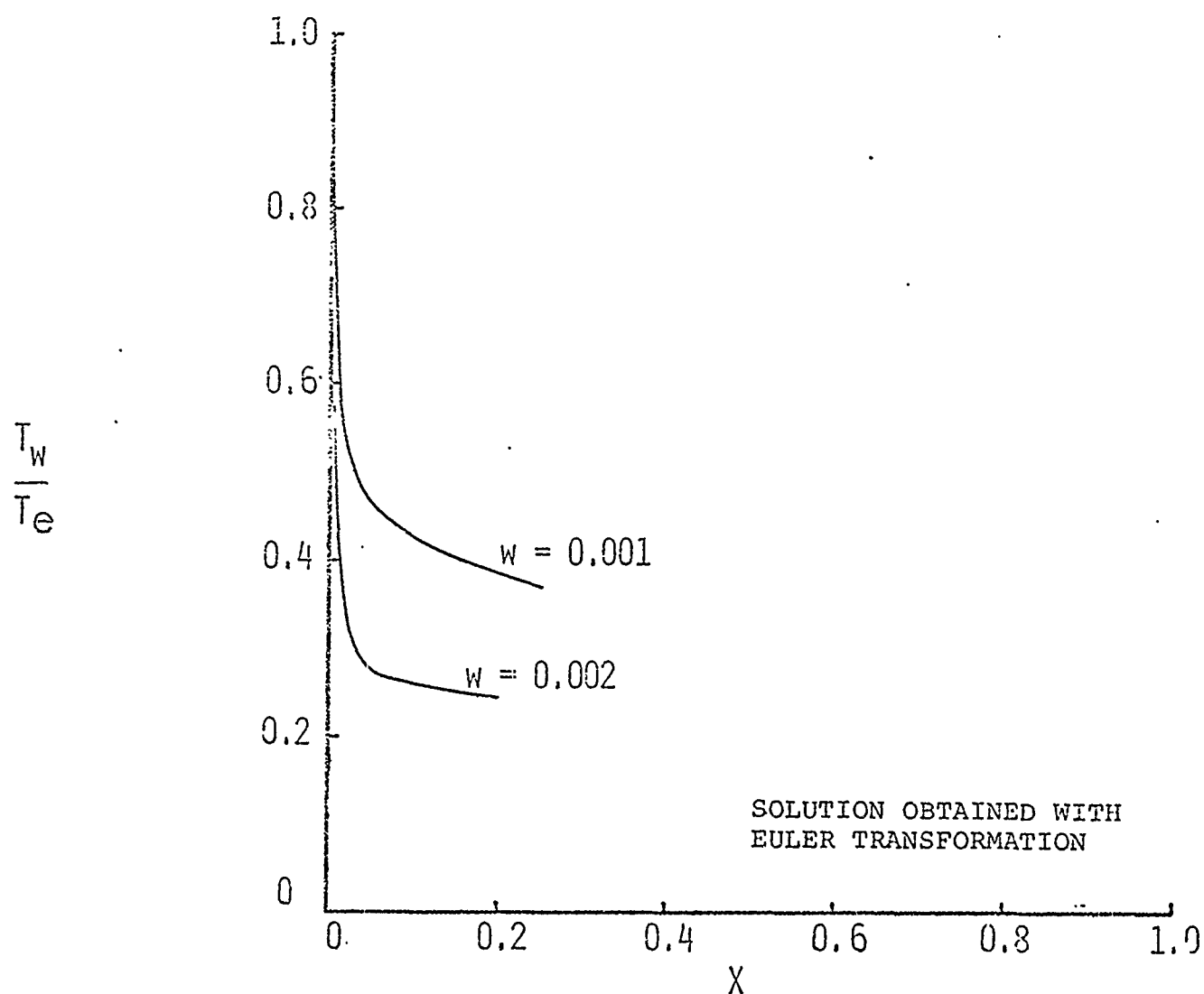FIGURE 19   FRICTION FACTOR OVER SUCTION SIDE OF THE AIRFOIL .

44

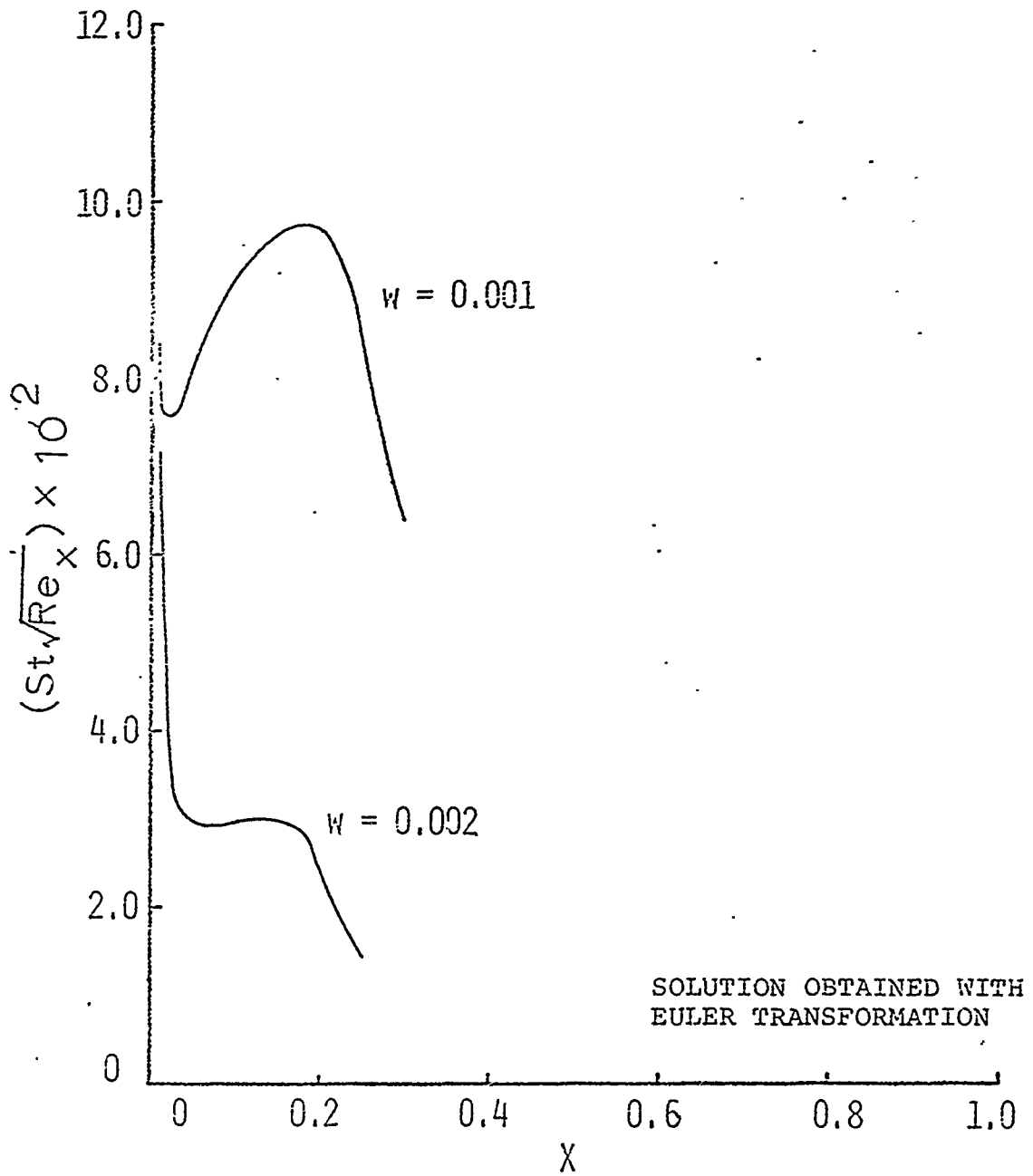FIGURE 20   WALL TEMPERATURE DISTRIBUTION OVER THE PRESSURE SIDE OF
THE AIRFOIL

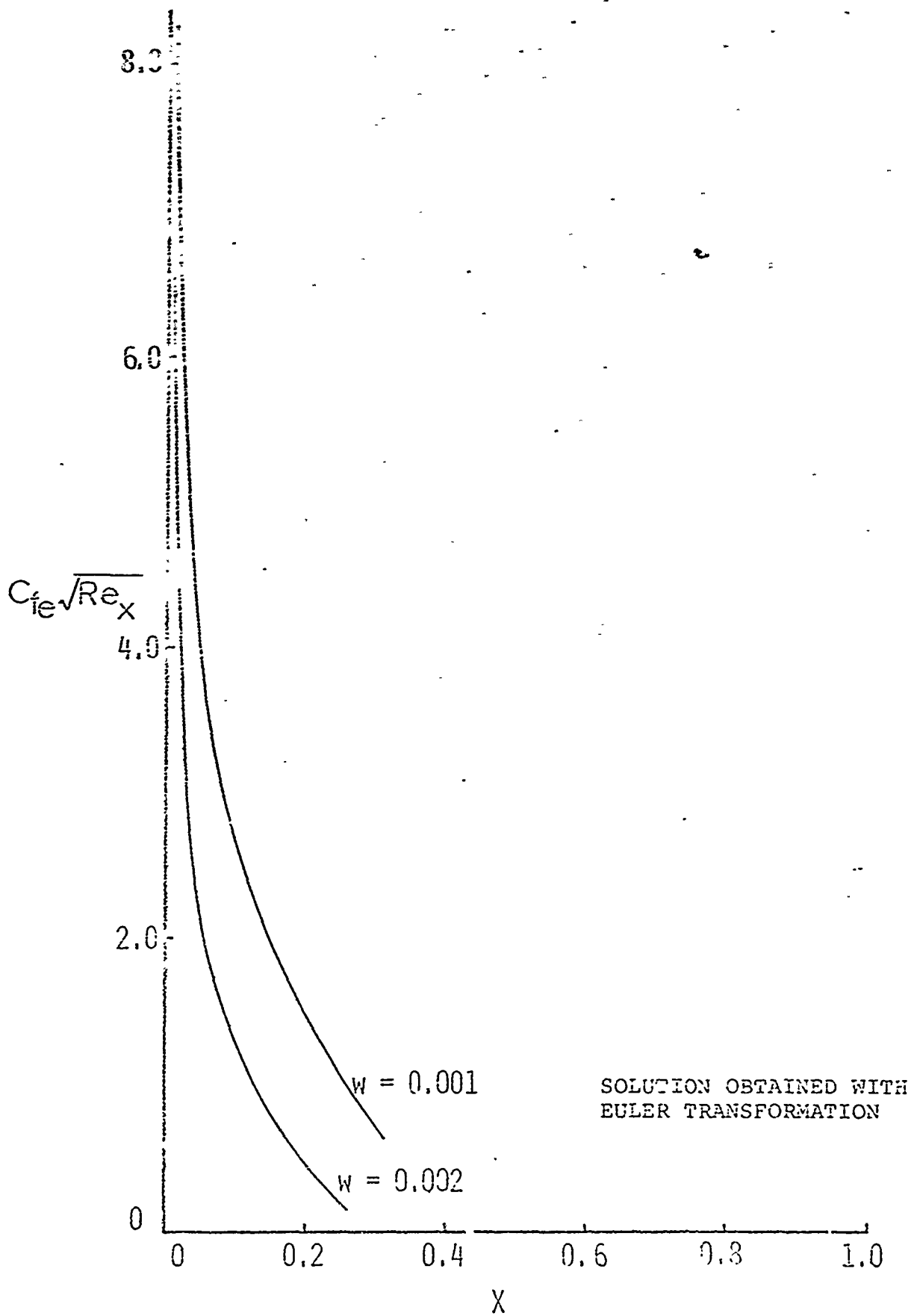FIGURE 21 HEAT TRANSFER OVER THE PRESSURE SIDE OF THE AIRFOIL

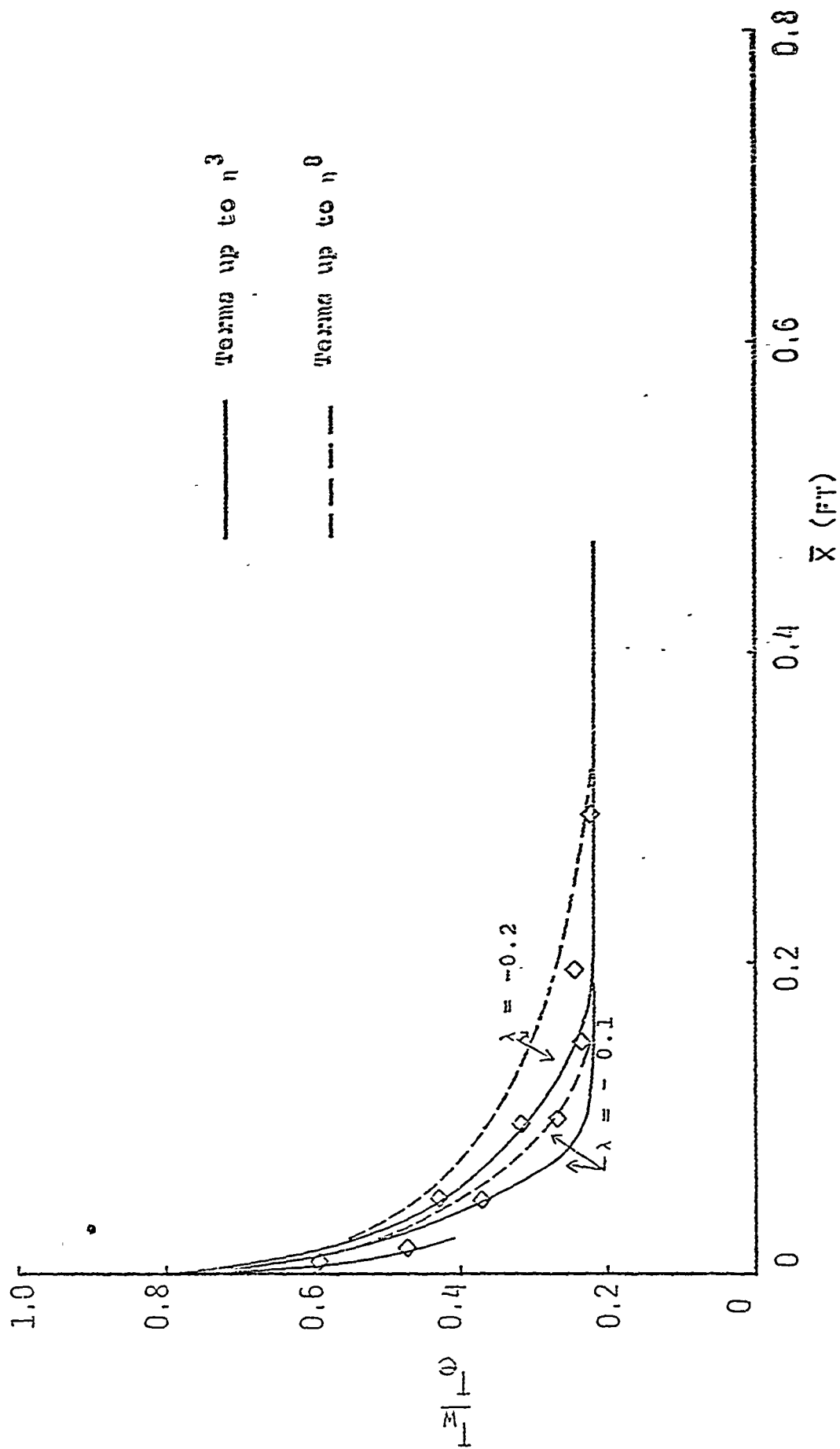FIGURE 22   FRICTION FACTOR OVER THE PRESSURE SIDE OF THE AIRFOIL

FIGURE 23   EFFECT OF INCLUSION OF HIGHER ORDER TERMS ON THE WALL
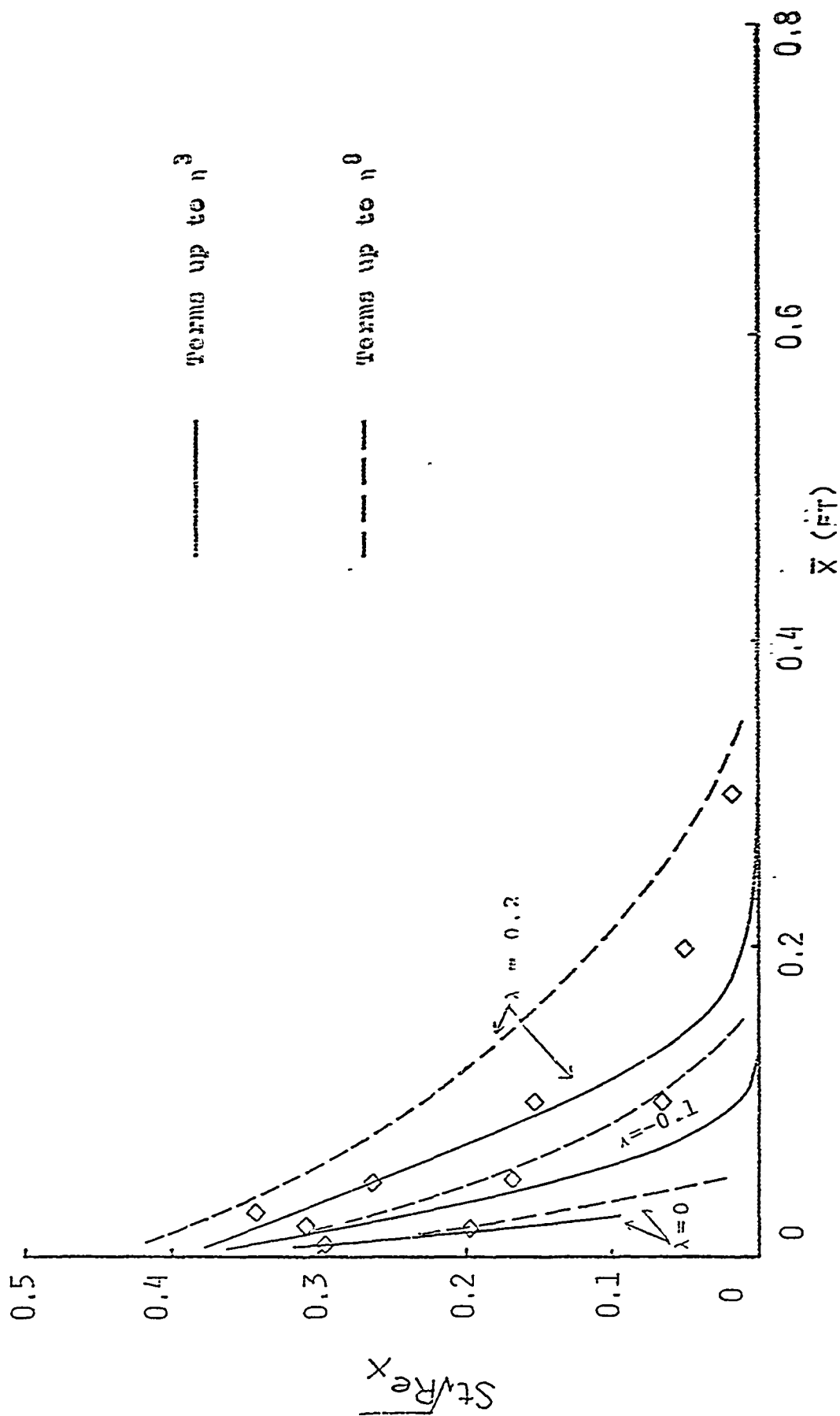TEMPERATURE DISTRIBUTION, W = 0.01

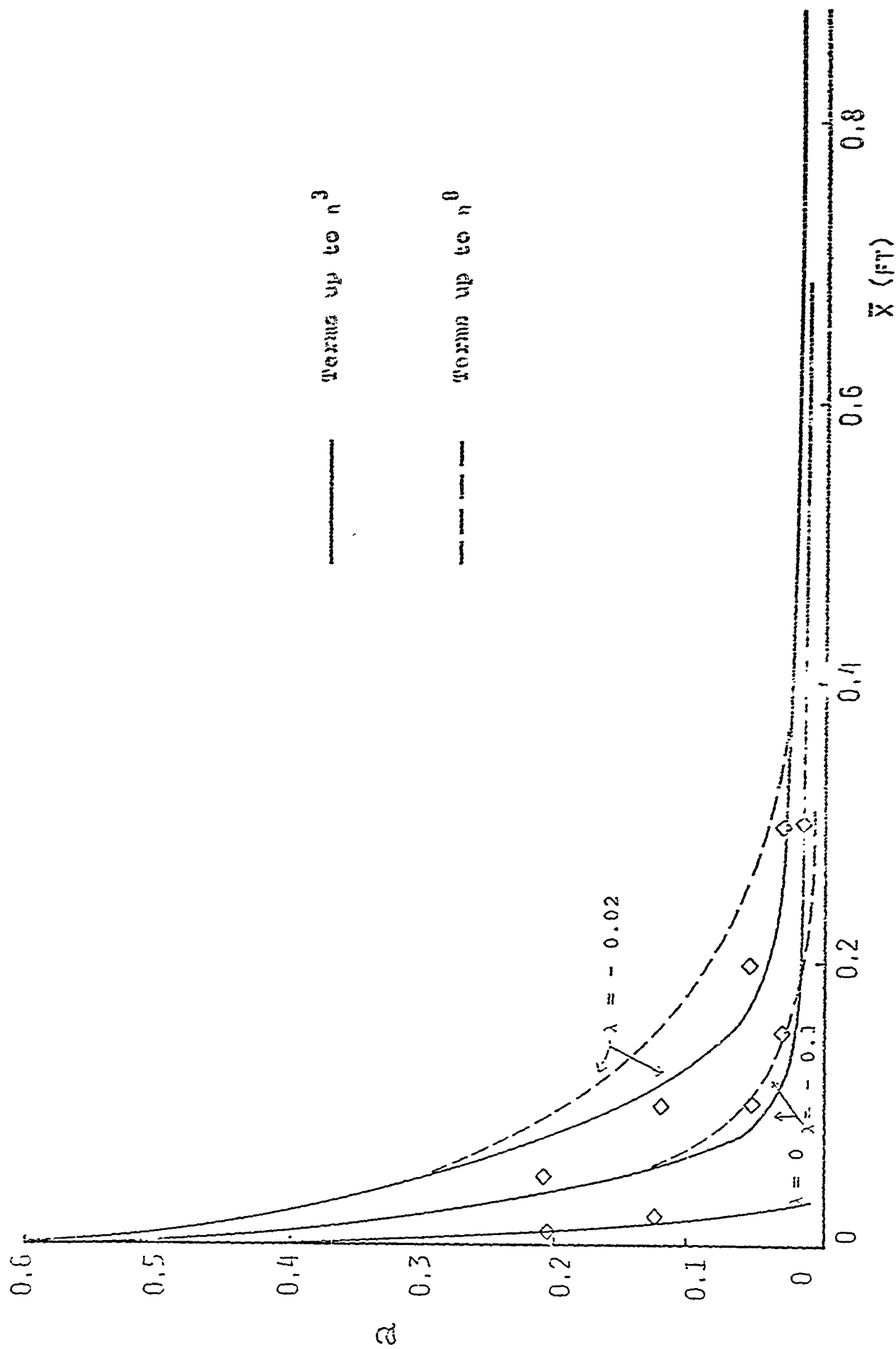FIGURE 24 EFFECT OF INCLUSION OF HIGHER ORDER TERMS
ON HEAT TRANSFER, $W = 0.01$.

49

FIGURE 25 EFFECT OF INCLUSION OF HIGHER ORDER TERMS
ON THE SHEAR STRESS PARAMETERS, W = 0.02